

**PREPARATION OF MOLECULARLY IMPRINTED  
POLYMERS FOR THE SOLID PHASE EXTRACTION OF  
PYRIDOXAL 5'-PHOSPHATE PRIOR TO HPLC  
DETERMINATION**

**A Thesis Submitted to  
the Graduate School of Engineering and Sciences of  
İzmir Institute of Technology  
in Partial Fulfillment of the Requirements for the Degree of**

**MASTER OF SCIENCE**

**in Chemistry**

**by  
Ömer ÖZYURT**

**July 2022  
İZMİR**

## ACKNOWLEDGMENTS

First and foremost, I would want to express my heartfelt gratitude and unending thanks to my supervisor, Prof. Dr. Ahmet E. EROĞLU, for providing me with the wonderful chance to work on this project. He has always been there with a smile whenever I got into difficulties, not only in science, but in life as well. My deepest thanks for his great counsel, tolerance, sympathy, and unwavering support.

I am grateful to Prof. Dr. Hasan ERTAŞ and Assoc. Prof. Dr. Levent PELİT for agreeing to participate on my thesis examination committee. I would also want to thank Assoc. Prof. Dr. Ezel BOYACI and Prof. Dr. Talal Shahwan for their valuable feedback on the study.

I would like also to thank to the Scientific and Technical Research Council of Turkey (TUBITAK) for financial support to this project (119Z862).

Additionally, I would like to thank my lab mates, particularly Hazal TOSUN and Yekta Arya ÖLÇER ALTINSOY, for their invaluable assistance.

My heartfelt gratitude goes to all of my IZTECH friends, especially Fikrican DİLEK, Yasemin BİLGİ, Dr. Murat DELMAN, Dr. Meltem KUTLUER, for their unwavering encouragement and companionship.

Finally, there are no words to convey how grateful I am to my family, my wife Elif GÜREL ÖZYURT, my mother Ayşe ÖZYURT, my father Halit ÖZYURT, and my sisters Melikenur ÖZYURT and Mervener ÖZYURT. I am eternally thankful to them for their unending love, patience, and encouragement to pursue my aspirations.

## ABSTRACT

### PREPARATION OF MOLECULARLY IMPRINTED POLYMERS FOR THE SOLID PHASE EXTRACTION OF PYRIDOXAL 5'-PHOSPHATE PRIOR TO HPLC DETERMINATION

Three different sorbent materials were prepared for solid phase extraction of pyridoxal phosphate (PLP), namely, carbon sphere based molecularly imprinted chitosan polymer (MICP), magnetite based molecularly imprinted chitosan polymer (MMICP) and silica (sol-gel) based molecularly imprinted polymer (IMIP). The sorbents were characterized by FT-IR, SEM, EDX, XRD, and TGA. The characterization data have shown that, the sorbents were relatively homogeneous, had very fast sorption kinetics and quantitative sorption over a wide range of analyte concentrations (1.0-100.0 mg/L). All the sorbents were found to be selective to PLP in presence of similar compounds; namely, pyridoxamine, nicotinic acid (vitamin B3), pyridoxal and 4-pyridoxic acid.

Sorption parameters for each sorbent were optimized. The optimum sorbent amount for 10.0 mL sample volume was found to be 5.0 mg for MICP and 10.0 mg for both MMICP and IMIP. A shaking duration of 30 min was employed in sorption experiments. Among the potential eluents, acetic acid solution (2%, v/v) has shown the best desorption performance for all three sorbents.

Method validation was investigated via spike recovery tests on water (ultra-pure, bottled and tap) and artificial serum samples. The recoveries obtained with water samples were greater than 96%, 92%, and 91% for MICP, MMICP, and IMIP, respectively. These results show the potential application of the methodologies for samples with relatively simple matrix. High recoveries (greater than 80%) were also obtained with artificial serum samples, whereas the use of matrix-matched calibration or internal standardization is suggested together with protein precipitation for biological samples with high protein content.

## ÖZET

### HPLC TAYİNİNDEN ÖNCE PİRİDOKSAL 5'-FOSFATIN KATI FAZ EKSTRAKSİYONU İÇİN MOLEKÜLER BASKILI POLİMERLERİN HAZIRLANMASI

Piridoksal fosfatın (PLP) katı faz ekstraksiyonu için karbon küre bazlı moleküler baskılanmış kitosan polimer (MICP), manyetit bazlı moleküler baskılanmış kitosan polimer (MMICP) ve silika (sol-jel) bazlı moleküler baskılanmış polimer (IMIP) olmak üzere üç farklı sorbent materyal hazırlandı. Sorbentler, FT-IR, SEM, EDX, XRD ve TGA ile karakterize edildi. Karakterizasyon verileri, sorbentlerin oldukça homojen olduğunu, çok hızlı sorpsiyon kinetiği ve geniş bir analit derişim aralığında (1.0-100.0 mg/L) kantitatif sorpsiyona sahip olduğunu göstermiştir. Tüm sorbentlerin, benzer moleküller olan piridoksamin, nikotinik asit (B3 vitamini), piridoksal ve 4-piridoksik asit varlığında PLP'ye seçici olduğu bulundu.

Her bir sorbent için sorpsiyon parametreleri optimize edildi. Seçilen numune hacmi (10.0 mL) için optimum sorbent miktarı MICP için 5.0 mg, MMICP ve IMIP için 10.0 mg olarak belirlendi. Sorpsiyon süresi 30 dakika olarak uygulandı. Potansiyel eluentler içinde en iyi desorpsiyon performansını tüm sorbentler için asetik asit çözeltisi (%2, v/v), gösterdi.

Yöntem doğrulaması, su (saf, şişe ve musluk) ve sentetik serum numunelerinde katım-geri kazanım testleri ile yapıldı. Sular için geri kazanım değerleri MICP, MMICP ve IMIP için sırasıyla %96, %92 ve %91'in üzerindedir. Bu sonuçlar, önerilen metodolojilerin nispeten basit matriksli numuneler için potansiyel uygulamasını göstermektedir. Benzer şekilde, sentetik serum için geri kazanım değerleri %80'in üzerinde olsa da yüksek protein içeriğine sahip biyolojik numuneler için protein çöktürme ile birlikte matriks-benzeşimli standart veya iç standart kalibrasyonu önerilmektedir.

# TABLE OF CONTENTS

LIST OF FIGURES .....	ix
LIST OF TABLES.....	xii
CHAPTER 1. INTRODUCTION .....	1
1.1. Vitamins.....	1
1.2. Vitamin B6.....	2
1.2.1. Vitamin B6 Levels in the Body.....	3
1.2.2. Determination Methods of Vitamin B6 .....	4
1.3. Solid Phase Extraction .....	5
1.3.1. Molecular Imprinting Technology .....	6
1.3.1.1. Types of Molecular Imprinting.....	8
1.3.1.1.1. Covalent Imprinting Method .....	8
1.3.1.1.2. Non-covalent Imprinting Method.....	9
1.3.1.1.3. Ionic/Metallic Imprinting Method .....	9
1.3.1.2. Green Synthesis of Molecularly Imprinted Chitosan Polymer .....	10
1.3.1.3. Magnetic Molecularly Imprinted Chitosan Polymer .....	10
1.3.1.4. Inorganic Molecularly Imprinting Polymer by Sol-Gel Process .....	11
1.4. The Aim of the Study.....	11
CHAPTER 2. EXPERIMENTAL STUDY .....	12
2.1. Reagents and Solutions .....	12
2.2. Optimization of HPLC-DAD Parameters .....	12
2.3. Synthesis of Carbon Sphere/Fe <sub>3</sub> O <sub>4</sub> based Molecularly Imprinted Chitosan Polymers .....	13
2.3.1. Synthesis of Chitosan.....	13

2.3.2. Synthesis of Carbon Sphere .....	13
2.3.3. Synthesis Fe <sub>3</sub> O <sub>4</sub> Particles .....	14
2.3.4. Preparation of Carbon Sphere Based Molecularly Imprinted Chitosan Polymer .....	14
2.3.5. Preparation of Fe <sub>3</sub> O <sub>4</sub> Based Molecularly Imprinted Chitosan Polymer .....	15
2.4. Synthesis of Inorganic Molecularly Imprinted Polymer by Sol-gel Process .....	15
2.5. Characterization Studies .....	16
2.5.1. Characterization of Chitosan .....	16
2.5.1.1. Infrared Spectroscopy .....	16
2.5.1.2. Degree of Deacetylation .....	17
2.5.1.2.1. Potentiometric Titration .....	17
2.5.1.2.2. Elemental Analysis .....	17
2.5.2. Characterization of the Sorbents .....	18
2.6. Sorption Studies .....	18
2.6.1. Binding Characteristic Assay .....	18
2.6.2. Selectivity Experiments .....	19
2.6.3. Effect of Sorption Time on the Extracted Amount of the Analyte .....	20
2.6.4. Effect of Sorbent Amount on the Extracted Amount of Analyte .....	20
2.6.5. Effect of Sample Volumes .....	21
2.7. Sorption Isotherm models .....	21
2.8. Desorption Studies .....	24
2.9. Method Validation .....	25
<b>CHAPTER 3. RESULTS AND DISCUSSIONS .....</b>	<b>26</b>
3.1. Optimization of Instrumental Parameters .....	26
3.2. Sorbent Characterization Studies .....	28

3.2.1	Characterization of Chitosan.....	28
3.2.1.1	Infrared Spectroscopy .....	28
3.2.1.2	Degree of Deacetylation of Synthesized Chitosan.....	28
3.2.2	Morphological Characterization of Carbon Sphere .....	30
3.2.3	Morphological Characterization of Fe <sub>3</sub> O <sub>4</sub> Nanoparticles .....	30
3.2.4	Characterization of Carbon Sphere Based Molecularly Imprinted Chitosan Polymer .....	32
3.2.5	Characterization of Fe <sub>3</sub> O <sub>4</sub> Based Molecularly Imprinted Chitosan Polymer .....	33
3.2.6	Characterization Sol-Gel Based Molecularly Imprinted Polymer .....	36
3.3	Sorption Studies.....	38
3.3.1	Binding Characteristic Assay.....	38
3.3.2	Selectivity Experiments .....	40
3.3.3	Effect of Sorption Time .....	44
3.3.4	Effect of Sorbent Amount.....	45
3.3.5	Effect of Sample Volume.....	46
3.4	Sorption Isotherm Models .....	47
3.5	Desorption Studies.....	54
3.6	Method Validation .....	55
CHAPTER 4. CONCLUSION .....		57
REFERENCES .....		59

# LIST OF FIGURES

<b><u>Figure</u></b>	<b><u>Page</u></b>
Figure 1.1: Vitamin B6 types, metabolism and related enzymes. Source: (Ueland et al. 2015). .....	4
Figure 1.2. Five primary types of molecular imprinting: (i) noncovalent, (ii) electrostatic/ionic, (iii) covalent, (iv) semicovalent and (v) ligand exchange. ....	7
Figure 2.1. Molecular structures of chitin and chitosan. ....	13
Figure 3.1. Chromatogram of standard solution containing (1) pyridoxamine, (2) nicotinic acid (vitamin B3), (3) pyridoxal, (4) pyridoxal phosphate and (5) 4-pyridoxic acid.....	26
Figure 3.2. Calibration plots for pyridoxamine, pyridoxal, nicotinic acid, 4-pyridoxic acid and pyridoxal phosphate. ....	27
Figure 3.3. FT-IR spectra of chitin and chitosan. ....	28
Figure 3.4. Potentiometric titration of synthesized chitosan with standardized NaOH solution. ....	29
Figure 3.5. SEM images of carbon sphere (magnification by: (a) 2500x times and (b) 5000x times. ....	30
Figure 3.6. SEM images of Fe <sub>3</sub> O <sub>4</sub> nanoparticles (magnification by: (a) 100000 times and (b) 200000 times). ....	31
Figure 3.7. EDX graph of Fe <sub>3</sub> O <sub>4</sub> nanoparticles. ....	31
Figure 3.8. X-ray diffraction patterns for Fe <sub>3</sub> O <sub>4</sub> nanoparticles and Fe <sub>3</sub> O <sub>4</sub> based molecularly imprinted chitosan polymer (MMICP). ....	32
Figure 3.9. SEM images of carbon sphere based molecularly imprinted chitosan polymer (MICP) (a and b) and non-imprinted chitosan polymers NICP (c and d); (a) magnified 1000 times, (b) magnified 2500 times, (c) magnified 1000 times and (d) magnified 2500 times. ....	33
Figure 3.10. SEM images of Fe <sub>3</sub> O <sub>4</sub> based molecularly imprinted chitosan polymer (MMICP): (a) magnified 25000 times and (b) magnified 50000 times.....	34
Figure 3.11. EDX graph of Fe <sub>3</sub> O <sub>4</sub> based molecularly imprinted chitosan polymer (MMICP). ....	34

<b><u>Figure</u></b>	<b><u>Page</u></b>
Figure 3.12. TGA thermogram of chitosan, Fe <sub>3</sub> O <sub>4</sub> nanoparticles and Fe <sub>3</sub> O <sub>4</sub> based molecularly imprinted chitosan polymer. ....	35
Figure 3.13. SEM images of (a and b) silica (sol-gel) based molecularly imprinted polymers and (c and d) non-imprinted polymers: (a) magnified 25000 times, (b) magnified 50000 times, (c) magnified 25000 times and (d) magnified 50000 times. ....	36
Figure 3.14. EDX graphs of (a) silica (sol-gel) based molecularly imprinted polymer and (b) non-imprinted polymer. ....	37
Figure 3.15. Sorption capacities of carbon sphere based MICP and NICP. ....	38
Figure 3.16. Sorption capacities of Fe <sub>3</sub> O <sub>4</sub> based MMICP and MNICP. ....	39
Figure 3.17. Sorption capacities of silica (sol-gel) based IMIP and INIP. ....	40
Figure 3.18. Sorption capacities of carbon sphere based MICP and NICP in the presence of pyridoxamine, nicotinic acid, pyridoxal and 4-pyridoxic acid. ....	40
Figure 3.19. Sorption capacities of Fe <sub>3</sub> O <sub>4</sub> based MMICP and MNICP in the presence of pyridoxamine, nicotinic acid, pyridoxal and 4-pyridoxic acid. ....	42
Figure 3.20. Sorption capacities of Silica (sol-gel) based IMIP and INIP in the presence of pyridoxamine, nicotinic acid, pyridoxal and 4-pyridoxic. ....	43
Figure 3.21. Effect of shaking time on the sorption of pyridoxal phosphate by carbon sphere based MICP, Fe <sub>3</sub> O <sub>4</sub> based MMICP and silica (sol-gel) based IMIP (n=3). ....	45
Figure 3.22. Effect of sorbent amounts on the sorption of pyridoxal phosphate by carbon sphere based MICP, Fe <sub>3</sub> O <sub>4</sub> based MMICP and silica (sol-gel) based IMIP (n=3). ....	46
Figure 3.23. Effect of sample solution volumes on the sorption of pyridoxal phosphate by carbon sphere based MICP, Fe <sub>3</sub> O <sub>4</sub> based MMICP and silica (sol-gel) based IMIP, sorbent amount 10.0 mg, shaking time 24 h, (n=3). ....	47
Figure 3.24. Nonlinear fit of isotherm models for sorption of pyridoxal phosphate by (a) MICP, (b) NICP, (c) MMICP, (d) NMICP, (e) IMIP and (f) INIP. ....	51

<b><u>Figure</u></b>	<b><u>Page</u></b>
Figure 3.25. Effect of eluent type on desorption of pyridoxal phosphate from MICP, MMICP and IMIP. ....	54

## LIST OF TABLES

<b><u>Table</u></b>	<b><u>Page</u></b>
Table 2.1. HPLC-DAD optimized parameters.....	12
Table 2.2. Some functional groups and their IR bands positions. (Source: Solomons and Fryhle 2000).....	16
Table 2.3. Extraction conditions used in binding characteristic assay. ....	19
Table 2.4. Experimental parameters employed for the investigation of the effect of sorption time on the sorption pyridoxal phosphate. ....	20
Table 2.5. Experimental parameters to analyze the effect of sorbent amount for sorption of pyridoxal phosphate. ....	21
Table 2.6. Experimental parameters used for the investigation of the effect of sample volume on the sorption of pyridoxal phosphate ....	21
Table 2.7. Experimental parameters used for the investigation of the effect of eluent type on the elution of pyridoxal phosphate. ....	24
Table 3.1. The line equations of the calibration curves, R <sup>2</sup> values and calculated LOD and LOQ values. ....	27
Table 3.2. Elemental analysis of synthesized chitosan by EDX.....	29
Table 3.3. Degree of deacetylation of chitosan by two methods.....	29
Table 3.4. The elemental composition of Fe <sub>3</sub> O <sub>4</sub> nanoparticles analyzed by EDX. ....	31
Table 3.5. The elemental composition Fe <sub>3</sub> O <sub>4</sub> based molecularly imprinted chitosan polymer analyzed by EDX. ....	34
Table 3.6. Elemental compositions of silica (sol-gel) based molecularly imprinted polymer (IMIP) and non-imprinted polymer (INIP). ....	37
Table. 3.7. Carbon sphere based MICP and NICP distribution coefficients, selectivity coefficients, and relative selectivity coefficients. ....	41
Table. 3.8. Fe <sub>3</sub> O <sub>4</sub> based MMICP and MNICP distribution coefficients, selectivity coefficients, and relative selectivity coefficients. ....	43
Table 3.9. Silica (sol-gel) based IMIP and INIP distribution coefficients, selectivity coefficients, and relative selectivity coefficients. ....	44
Table 3.10. Summary of models' coefficients and constants for MICP and NICP.....	48

<b><u>Table</u></b>	<b><u>Page</u></b>
Table 3.11. Summary of models' coefficients and constants for MMICP and NMICP.....	49
Table 3.12. Summary of models' coefficients and constants for IMIP and INIP.....	50
Table 3.13. Chi-tests results of MICP and NICP.....	52
Table 3.14. Chi-tests results of MMICP and MNICP.....	52
Table 3.15. Chi-tests results of IMIP and INIP. ....	53
Table 3.16. Recovery results obtained with the proposed method (n=3). ....	56

# CHAPTER 1

## INTRODUCTION

### 1.1. Vitamins

It is widely known that vitamins are essential for health, and if the one eats the right food a decent supply is guaranteed. Vitamins help your body grow and work the way it should. There are 13 essential vitamins: vitamins A, C, D, E, K, and the B vitamins (thiamine, riboflavin, niacin, pantothenic acid, biotin, B6, folate, and B12). In order to help keep the body functioning well, vitamins have multiple tasks. Some vitamins acts preventive agents against infections and keep the nerves healthy, while others play important role for body to receive nutritional energy or help with blood clotting. Based on their solubility, they can be classified as: fat-soluble vitamins and water-soluble vitamins.

The fat-soluble vitamins are stored in the body's fatty tissue. The four fat-soluble vitamins are vitamins A, D, E, and K. These vitamins are absorbed more easily by the body in the presence of dietary fat. Vitamin A plays an important role in preserving vision, immune function, body growth and hair growth (Kongsbak et al. 2008). Vitamin D has various functions and activities in bone maintenance and immune system regulations (Prietl et al. 2013) The essential objective of vitamin E is to operate as an antioxidant, reduce oxidative damage and preserve fatty acids from free radicals in cell membranes (Burton et al. 1983). And Vitamin K plays a vital role in blood clotting; moreover, it has other roles, such as promoting bone integrity and working to reduce blood vessel calcification, thereby lowering the risk of cardiovascular diseases (Vermeer 2012).

Vitamin C and the vitamins B1, B2, B3, B5, B6, B9, B12 are soluble in water. Contrary to fat soluble vitamins, water soluble vitamins are not stored in the body and their excess amounts are eliminated by urinary excretion. While the body maintains a limited supply of these vitamins, they must be taken on a daily basis to reduce deficiencies in the body. The only water-soluble vitamin that can be processed for several years in the liver is cobalamin (vitamin B12). Thiamine (vitamin B1) acts as a coenzyme in the body (Farquharson and Adams 1976). This refers to all of its active forms, but the most important one is thiamine pyrophosphate. For example, it helps turn food into energy, and

leads to the formation of sugar (Fattal-Valevski 2011). Riboflavin (vitamin B2) operates as a coenzyme in numerous chemical reactions. It is also involved, as thiamine, in the transformation of nutrients into energy (Medicine 1998). Niacin (vitamin B3) acts as a coenzyme in the body, plays an essential part in cell processes, and works as an antioxidant, much like the other B vitamins. One of its most vital duties is to control the production of energy from glucose, a biochemical mechanism called glycolysis (sugar) (Medicine 1998). Pantothenic acid (vitamin B5) is needed for the production of coenzyme A, which is essential for the synthesis of lipids, amino acids, steroid hormones, neurotransmitters and numerous other significant substances (Tahiliani and Beinlich 1991). Vitamin B6 functions as a coenzyme in various chemical reactions, much as other B vitamins. It is involved in the production of red blood cells as well as the metabolism of energy and amino acids. The vitamin molecule the body uses to store carbohydrates is also required for the release of glucose (sugar) from glycogen. Vitamin B6 also allows white blood cells to develop and helps the body to synthesize multiple neurotransmitters (Spinneker et al. 2007). Similarly to other vitamins in vitamin B family, Biotin (vitamin B7) acts as a coenzyme. It is a cofactor for five carboxylase enzymes that are involved in carbohydrate digestion, fatty acid production, and gluconeogenesis. For example, it plays an important function in the synthesis of fatty acids, the formation of glucose and the digestion of amino acids (Lanska 2012). Folic acid or folate (vitamin B9) functions as a coenzyme and is important for the metabolism of cell growth, DNA production and amino acids. It is very crucial during cycles of fast cellular division and formation, including in pregnancy and childbirth (Medicine 1998). In addition to being a coenzyme, vitamin B12 has crucial role in brain functioning. For instance, it helps to sustain brain health and development, neurological function, and red blood cell production (Ueland et al. 2017). It is also very important for the energy conversion of protein and fat and is vital for the cell division process and DNA replication (Medicine 1998). Vitamin C does not function as a coenzyme, unlike B vitamins; however, it is a cofactor of prolyl hydroxylase, an enzyme that plays a significant role in collagen synthesis. Antioxidant defenses, collagen formation and immune function are the basic duties of vitamin C (Padayatty et al. 2003).

## **1.2. Vitamin B6**

Vitamin B6 is a part of the "vitamin B" essential food group and is a general term that refers to six compounds that can be converted into one another (Ueland et al. 2015).

Of these six compounds, pyridoxine (PN), pyridoxal (PL) and pyridoxamine (PM) are the three main forms (Fig. 1.1). Other forms, pyridoxine 5'-phosphate (PNP), pyridoxal 5'-phosphate (PLP) (pyridoxal phosphate), and pyridoxamine 5'-phosphate (PMP) are the three main forms phosphatized. Pyridoxine is given as a vitamin B6 supplement. Pyridoxine 5'-phosphate, its active form, acts as a coenzyme in many enzyme reactions that take place in amino acid, glucose and lipid metabolism. Pyridoxal 5'-phosphate is the metabolically active coenzyme form of vitamin B6, while PL is the carrier form that can pass through biological membranes. 4-pyridoxide acid (PA) is the catabolite of PN used as a supplement. Pyridoxal (PL), PN and PM are phosphorylated with pyridoxal kinase (PDXK) to PLP, PNP and PMP, respectively. Pyridoxine 5'-phosphate (PNP) and PMP are oxidized to PLP by pyridoxamine 5'-phosphate oxidase (PNPO). Pyridoxal 5'-phosphate (PLP) in the liver binds to albumin and enters the circulation to reach the tissues. Before PLP is taken into the cell, it is dephosphorylated to PL with non-tissue specific alkaline phosphatase (Sharma et al. 2014) or intracellular enzyme pyridoxal phosphatase (PDXP). In addition, 4-pyridoxic acid (PA), the catabolite excreted in urine, is synthesized with the help of aldehyde oxidase (AOX) by the irreversible oxidation of PL (Ueland et al. 2017).

### **1.2.1. Vitamin B6 Levels in the Body**

The human body cannot produce and store B6; therefore, a daily resource is required. Foods containing vitamin B6 are fortified breakfast cereals, pork, turkey, beef, banana, chickpeas, dark chocolate, potatoes, pistachios. In 1998, The Institute of Medicine (IOM) recommends the daily intake of vitamin B6 in the range of 1.0-1.3 mg for women and men aged 14 and over. In addition, a PLP value lower than 10 nmol.L<sup>-1</sup> in blood indicates a vitamin B6 deficiency. Vitamin B6 deficiency may result in seizures in young people. In adults with severe deficiency, rash and mental state changes are usually seen. Also, clinical deficiency may include normocytic anemia, a nonspecific pruritic rash, and swelling of the mouth and tongue. Depression is also associated with severe B6 deficiency. In addition, individuals with a PLP value higher than 151 nmol.L<sup>-1</sup> in the blood are considered to have a high vitamin B6 level (Wikipedia 2021,10 January, 15:35 UTC).

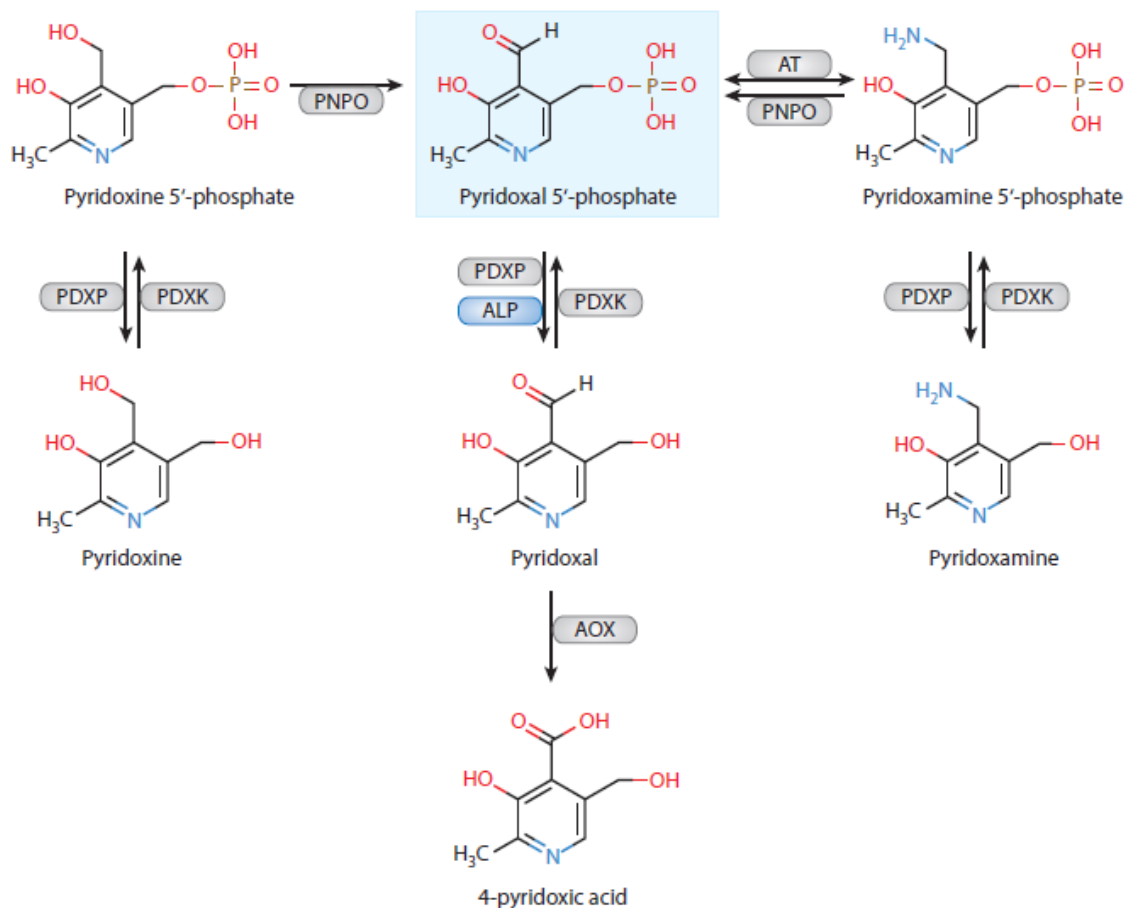


Figure 1.1: Vitamin B6 types, metabolism and related enzymes. Source: (Ueland et al. 2015).

High levels of sugar in the blood cause the formation of advanced glycation end products (AGEs) which play a significant role in the growth of complications such as nephropathy, neuropathy, retinopathy and atherosclerosis related to diabetes (Rhee and Kim 2018). Previous research has found that the PMP and PLP forms of vitamin B6 suppress the production of AGEs (Goh and Cooper 2008; Nakamura and Niwa 2005).

### 1.2.2. Determination Methods of Vitamin B6

For vitamin B6 determination, the high performance liquid chromatography (HPLC) method is preferred. All forms of vitamin B6 are determined using this approach (Mann et al. 2019). A semicarbazide based fluorometric technique for measuring pyridoxal phosphate (PLP) in whole blood, red cells, and plasma has been developed. When excited at 380 nm, the semicarbazone of PLP emits strongly at 460 nm (Srivastava and Beutler 1973). For quantifying the key vitamin B6 vitamers, pyridoxal

and pyridoxal phosphate (PLP), and 4-pyridoxic acid (4-PA), in plasma, a quick and accurate high-performance liquid chromatographic technique was created. The metabolites and 4-pyridoxic acid (PA) were extracted with 0.8 mol.L<sup>-1</sup> perchloric acid from plasma. The separation of the vitamin metabolites was carried out using an ODS R-P column and a mobile phase comprising 0.1 mol.L<sup>-1</sup> potassium dihydrogen phosphate, 0.1 mol.L<sup>-1</sup> sodium perchlorate, and 0.5 g.L<sup>-1</sup> sodium bisulfite adjusted to pH: 3.0, at a flow rate of 1.0 mL.min<sup>-1</sup>. This approach uses derivatization with sodium bisulfite in the mobile phase to detect PLP in plasma with great sensitivity (Kimura, Kanehira, and Yokoi 1996).

Separation (and/or preconcentration) of target compounds from biological, pharmacological, environmental, and dietary matrices is often the sample preparation phase. Extraction is typically necessary prior to chromatographic methods to remove analytes from interfering matrix components and enrich them prior to analysis.

### **1.3. Solid Phase Extraction**

Solid phase extraction (SPE) is an extraction method where compounds which are suspended or dissolved in a liquid phase are extracted from other substances in the mixture matrices according to their physical and chemical characteristics. Solid phase extraction methods have been used by analytical laboratories in order to isolate the analyte from the matrix and/or pre-concentrate it prior to instrumental analysis. To isolate the relevant analytes from a wide range of matrices, such as urine, blood, water, beverages, and other biological fluids, solid phase extraction may be used (Augusto et al. 2013; Hennion 1999).

SPE divides a mixture into desirable and unwanted components by utilizing the affinity of solutes that are dissolved or suspended in a liquid (referred to as the mobile phase) for a solid through which the sample is passed (referred to as the stationary phase). As a result of extraction, only the analyte of interest or unwanted impurities in the sample are separated by the solid phase. Based on whether it includes the analytes or undesired impurities, the fraction that passes through the solid phase is gathered or eliminated. If the analytes are in the solid phase, they can then be extracted by washing the solid phase with a suitable eluent (Buszewski and Szultka-Mlynska 2012).

Insufficient recovery of required analytes by SPE could be possible due to non-exhaustive extraction or incomplete elution. Non-exhaustive extraction mainly is due to

low affinity of the analyte to the extractive phase, high matrix-analyte interaction, and small breakthrough volumes. The other parameter effecting analyte recoveries is selection of the eluent with sufficient strength to ensure the completion of the desorption process (Raeke et al. 2016). SPE comes in a variety of phases. The majority of them rely on ionic, hydrophobic, or polar interactions. Their selectivity is low, and the analyte of interest frequently co-elutes with interfering chemicals. The most highly selective phases accessible today are Molecularly Imprinted Polymers. This method allows for less interference during the elution stage and greater recoveries in chromatography analysis even at low levels.

### **1.3.1. Molecular Imprinting Technology**

Molecular imprinting is a technique with predetermined selectivity and high affinity to create template-shaped cavities in polymer bulk (Chen et al. 2016). This concept is based on the method used for substrate recognition by enzymes, that is called the "lock and key" model. In 1931, Polyakov first suggested the idea of molecular imprinting as "uncommon adsorption properties of silica particles developed using a unique synthesis procedure" (Chen et al. 2016). After Polyakov's groundbreaking work in the 1930s using silica matrices, a large attention has drawn from the scientific community. The rapid advance of the development, planning, characterization and application of molecularly imprinted polymers (MIPs) in recent years has represented the steady maturation of molecular imprinting technology (Chen et al. 2011). Especially in comparison to other recognition systems, MIPs have gained widespread attention and have been attractive in many areas, such as purification and isolation, chemo/biosensing, artificial antibodies, drug distribution, and catalysis and degradation, due to their high mechanical properties and degradation, which have three key special features of structure predictability, recognition precision and usage universality (Chen et al. 2011). MIPs are an efficient way for target analytes to be isolated or pre-concentrated from a complex matrix prior to analysis (Hashim et al. 2014).

The molecular imprinting method includes the polymerization of a functional monomer along a molecular template and a cross-linker (Hongyuan and Row 2006). In this method, between a preferred template molecule and a corresponding functional monomer, template-monomer interactions are accomplished. The type of the template-monomer interaction defines the form of molecular imprinting, as shown in Fig 1.2.

A template, a functional monomer, a cross-linker, a polymerization initiator and a solvent (porogen) are the required components of a standard MIP synthesis process. Various attempts have been made to develop MIPs with unique properties, since many variables, such as the form and quantity of monomer, cross-linker, initiator and solvent, and the time and temperature of the polymerization process, influence the polymerization reaction. The "three-elements of molecular imprinting" include, as known, template molecules, functional monomers and cross-linkers, that should be discussed in detail (Chen et al. 2016).

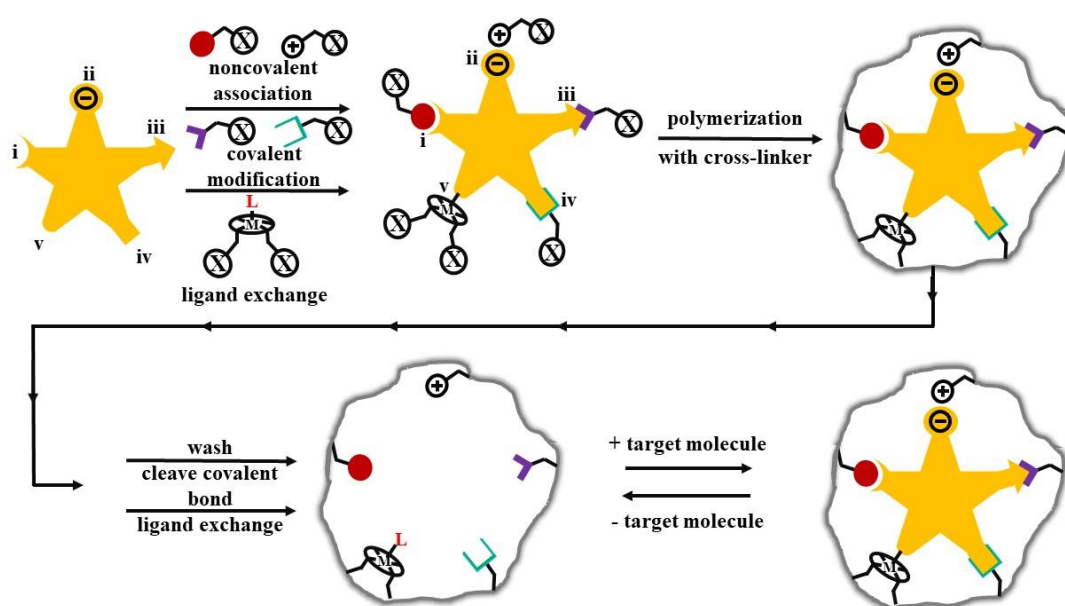


Figure 1.2. Five primary types of molecular imprinting: (i) noncovalent, (ii) electrostatic/ionic, (iii) covalent, (iv) semicovalent and (v) ligand exchange.

As described above, molecular imprinting helps to create artificial receptors in polymeric materials for a specific target molecule. The target molecule serves as a template upon which a cast-like shell is arranged and co-polymerized to construct combining and cross-linking monomers. In substance, a molecular memory is imprinted based on its own physical and chemical shape in the polymer network which is now able to selectively bind the target molecule (Hashim et al. 2014).

In the presence of target molecule that will be removed later to leave behind its complementary cavities, polymerization of functional monomers is involved in the process. With these complementary cavities, these polymers are expected to have interest for the target molecules and be used in applications of molecular separations, catalysis,

or chemical sensing. Selectivity is therefore determined by the covalent and noncovalent interactions between the target analyte and the monomer functional groups.

The cross-linker performs three main functions in an imprinted polymer; firstly, it is essential for regulating the morphology of the polymer matrix, whether it is gel-type, macroporous or microgel powder. Moreover, it helps to stabilize the attachment site imprinted. Lastly, the polymer matrix imparts mechanical flexibility. High cross-link proportions are typically favored from a polymerization point of view in order to reach indefinitely porous materials and be able to produce materials with sufficient structural integrity (Hongyuan and Row 2006).

### **1.3.1.1. Types of Molecular Imprinting**

The selectivity of the MIPs is evaluated by the covalent, noncovalent and ionic interactions between the target analyte and functional groups of the monomer. The proper use of functional monomers is another effective option for complementary relationships with the target analyte and substrates to select the type of molecular imprinting (Hongyuan and Row 2006). Details of different types of interactions between analyte and substrate are given below.

#### **1.3.1.1.1. Covalent Imprinting Method**

Functional monomers can be covalently attached to the template molecule, resulting in the formation of a polymerizable derivative of the template molecule. Because covalent bonding are more stable, covalent imprinting techniques should produce a more uniform population of binding sites, and there have been studies indicating that this may be the case. Furthermore, the yield in binding sites per template molecule employed (imprinting efficiency) should be larger than with noncovalent methods (Haupt and Mosbach 2000). The target analyte molecule is covalently bound to the functional monomers in covalent imprinting and are then polymerized together. The target analyte molecule is separated from the polymer matrix, leaving a void shaped like the target analyte molecule. The binding sites will engage with the target molecule upon rebinding with the original molecule, restoring the covalent bonds (Burnouf and Radosevich 2001; Wulff 1982). The advantages of covalent imprinting; more durable and rigid types of interactions, the stable template-monomer complex during the

polymerization process and more homogeneous binding sites. The disadvantages are strong covalent interactions results in slow binding and rebinding and difficult to remove the template (Nur Hasanah et al. 2021).

#### **1.3.1.1.2. Non-covalent Imprinting Method**

Polymers and imprinted molecules are spontaneously and neatly structured via molecular interaction forces in non-covalent techniques. Hydrogen bonds, dipole dipole interactions, and induced dipole forces may include the factors acting in this technique (Alexander et al. 2006). Because of simple processing and the large array of functional monomers which can be attached to the target molecule, this process is the most commonly employed method in MIP preparation. Of all functional groups, attributed to its ability to interact with other functional groups, methacrylic acid is by far the most widely used monomer (Andersson et al. 1984; Kempe et al. 1995). The advantages of non-covalent imprinting method are fast, straightforward and flexible binding interactions, easy template-monomer complex preparation, easy template removal and resulting high affinity binding, greater affinity and selectivity to site. Non-covalent interactions are sensitive to disruptions (Nur Hasanah et al. 2021).

#### **1.3.1.1.3. Ionic/Metallic Imprinting Method**

Ionic or metallic imprinting, requiring metal ions, functions as an alternative to strengthening the relationship of the template molecule and functional monomer in water (Yavuz et al. 2005). Metal ions usually act during the imprinting procedure as a mediator. Ionic imprinting, which uses metal ions, is a method for improving template molecule and functional monomer interactions in water. In the presence of a metal ion, cross-linking polymers generate a matrix capable of metal binding (Xu et al. 2015). This method yielded polymers that were used in the development of ion selective sensors, metal ion pre-concentration, and remediation investigations. The strength of the interaction can be influenced by the oxidation state of the metal ion and the properties of the ligand, comparable to the strength of a covalent bond (Sajini and Mathew 2021).

### **1.3.1.2. Green Synthesis of Molecularly Imprinted Chitosan Polymer**

Chitosan is a biopolymer produced from chitin obtained from marine sources. It is formed when chitin is deacetylated either chemically with the help of concentrated basic solution or enzymatically with chitin deacetylase. Chitosan has several qualities; it is non-toxic, biodegradable, biocompatible, anti-allergic, anticoagulant, antifungal, and antibacterial. All of these features make it feasible to employ chitosan in a broad array of applications, including pharmaceutical, foodstuff, and sensors. Because of its film-forming capabilities, biodegradability, and non-toxicity, chitosan has been widely exploited in the development of MIPs (Karrat et al. 2020; Karrat et al. 2022; Kharroubi et al. 2021).

Numerous supports are applied in the imprinting technique, specifically those with a great surface area and high porosity, such as carbon nanotubes, graphene oxide, silica nanoparticles, quantum dots, and carbon spheres (CS). Carbon sphere has attracted widespread interest as a sophisticated main support for surface imprinting due to excellent properties such as cost-effective starting material, ecologically responsible synthesizing method, functionally viable micro/nanostructure, superior biocompatibility and chemical inertness (Liu et al. 2016; Qin et al. 2016).

Biopolymers and their derivatives have a mechanically stable three-dimensional structure and, depending on the adaptation of the shape, size and functional group, the template molecules are trapped in specific sites of molecular recognition and then imprinted on the structure of the polymer (Zheng and Yoshikawa 2015).

### **1.3.1.3. Magnetic Molecularly Imprinted Chitosan Polymer**

Chitosan has been recognized as a significant polymer in the development of molecularly imprinted polymers (MIPs) and ion-imprinted polymers (IIPs) as well as their composites. Due to several superior features such as fast and effective binding to target analytes, shorter pre-treatment time, reversible and controllable flocculation, and easy separation of polymers from sample matrix using an external magnet, magnetic molecularly imprinted polymers (MMIPs) have gotten more attention.

Co-precipitation is the most common technique for generating  $\text{Fe}_3\text{O}_4$  nanoparticles. This approach involves combining Fe(III) and Fe(II) ions in highly basic

solutions at ambient temperature or raised temperature in a 1:2 molar ratio (Çiftçi and Coşkun 2020).

#### **1.3.1.4. Inorganic Molecularly Imprinting Polymer by Sol-Gel Process**

The sol-gel technique is a method for producing oxidized materials in which a sol is created by hydrolysis in the liquid phase and subsequently transformed into a gel. When more than two reactants are employed, the sol-gel process can yield a product with a high degree of purity as well as a uniformly mixed result. Furthermore, the product can be made utilizing the sol-gel method at relatively low temperatures. As a result, a variety of structures, such as thin membranes, fibers, and nano-size materials, can be formed. While organic monomers are easier to work with than inorganic monomers, almost all MIP research has been done using them. As a result, there has been limited study on MIPs created with inorganic monomers (Shin 2013).

### **1.4. The Aim of the Study**

The aim of this thesis is to prepare a new solid phase extraction sorbents for the specific recognition of pyridoxal 5'-phosphate (PLP) before chromatographic determination. To that end, several types of molecular imprinted polymers were produced against PLP. In terms of binding capability, selectivity, sorption time, sorbent amount and sample volume, the sorption performances of MIPs and NIPs with different preparation techniques were studied. The optimization of working parameters for PLP sorption by the sorbents was performed as: sorption capacity, shaking time, amount of sorbent, sample volume successive loading of PLP. The sorbents selectivity for PLP was investigated in the presence of pyridoxamine, nicotinic acid, pyridoxal and 4-pyridoxic acid. SEM, XRD and EDX were used to characterize the materials. After the sorbents were characterized, their sorption characteristics were evaluated under PLP-optimized conditions.

## CHAPTER 2

### EXPERIMENTAL STUDY

#### 2.1. Reagents and Solutions

All chemicals used were of analytical reagent purity. Throughout the study, ultra-pure water (18.2 MΩ.cm) was used. Pyridoxal 5'-phosphate hydrate (PLP) (98%), pyridoxamine dihydrochloride (analytical grade, 98%), pyridoxal hydrochloride (HPLC grade, 99%), nicotinic acid (98%), 4-pyridoxic acid (98%), chitin (practical grade, powder), sodium hydroxide (NaOH, pellets), iron(II) sulfate heptahydrate (FeSO<sub>4</sub>·7H<sub>2</sub>O), methanol (HPLC grade, 99.9%), trifluoroacetic acid (TFA) (99%), (3-Aminopropyl) triethoxysilane (APTES) (99%) and tetraethyl orthosilicate (TEOS) (98%) were purchased from Sigma-Aldrich. Tetrahydrofuran (THF) and iron(III) chloride hexahydrate (FeCl<sub>3</sub>·6H<sub>2</sub>O) were purchased from Merck. D(+) glucose monohydrate, acetic acid and ethanol (99.9%) were purchased from Isolab Chemicals.

#### 2.2. Optimization of HPLC-DAD Parameters

For the HPLC-DAD optimization process, 100.0 mg.L<sup>-1</sup> of pyridoxal phosphate (PLP) and 4-pyridoxic acid stock solutions were prepared separately in deionized water and stored in 4 °C in refrigerator. Additionally, 100.0 mg.L<sup>-1</sup> of pyridoxamine and nicotinic acid stock solutions were prepared separately in methanol and stored in -18 °C in refrigerator. Standard calibration solutions used in HPLC and samples used in extraction studies were prepared daily with suitable dilutions of stock solutions.

Table 2.1. HPLC-DAD optimized parameters.

Column	Waters Spherisorb ODS2 (5 μm 4.6x250mm)
Mobile phase	95% Water(0.2% TFA): 5% Methanol
Column temperature	30°C
Sample injection volume	20 μL
Flow Rate	1.0 mL/min
Standard Concentrations	0.025, 0.05, 0.1, 0.25, 0.5, 1, 5, 10 mg/L

Agilent 1200 Series HPLC with Diode Array Detector was used in all analyses performed. The optimized chromatographic parameters are shown in Table 2.1.

## 2.3. Synthesis of Carbon Sphere/Fe<sub>3</sub>O<sub>4</sub> based Molecularly Imprinted Chitosan Polymers

### 2.3.1. Synthesis of Chitosan

Chitosan is synthesized via deacetylation of chitin. At temperatures over 100 °C, the acetamide groups of chitin are hydrolyzed using concentrated NaOH or KOH (40–50%, w/v) under inert atmosphere. Firstly, in a 1L three-necked round bottomed flask with a reflux condenser linked to its middle neck, 15.0 g of chitin was treated with 720 mL of 40.0% (w/v) aqueous NaOH solution. N<sub>2</sub> gas was bubbled into the mixture from one side arm to generate an inert environment in the reaction medium and to regulate the temperature, a thermometer was attached to the other side arm. At 115 °C, constant reflux was established and maintained for 6 hours. After deacetylation, the alkaline solution was cooled down to ambient temperature and chitosan flakes are filtered and washed until neutral filtrate obtained. Finally, the obtained chitosan flakes were dried for 2 h at 60°C before use (Boyacı et al. 2010). Figure 2.1 show the molecular structures of chitin and chitosan.

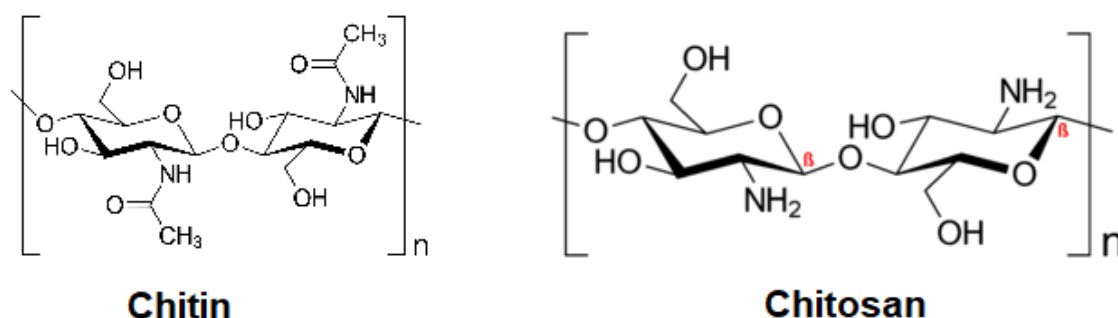


Figure 2.1. Molecular structures of chitin and chitosan.

### 2.3.2. Synthesis of Carbon Sphere

Carbon sphere (CS) was synthesized from glucose as the carbon source by green and simple hydrothermal method reported in a previous study (Ostovan et al. 2018). Briefly, glucose (1.8 g) was dissolved in deionized water (25.0 mL) with magnetic stirring

to obtain a clear solution. The solution was transferred into a 25.0 mL stainless-steel PTFE lined autoclave. It was then sealed and heated for 8 h at 180 °C. After heating, the reactor was let to cool down to ambient temperature. The obtained brown particles were filtered and washed with deionized water and ethanol. To eliminate the remaining ethanol, the product was dried at 60 °C for 12 h.

### **2.3.3. Synthesis Fe<sub>3</sub>O<sub>4</sub> Particles**

Magnetite (Fe<sub>3</sub>O<sub>4</sub>= FeO·Fe<sub>2</sub>O<sub>3</sub>) nanoparticles were prepared via the titration of FeCl<sub>3</sub> and FeSO<sub>4</sub> with NaOH (Díaz-Hernández et al. 2018). Briefly, 100.0mL 0.5 M FeCl<sub>3</sub>·6H<sub>2</sub>O solution and 50.0 mL 0.5 M FeSO<sub>4</sub>·7H<sub>2</sub>O solution were mixed in a 500 mL beaker and 50.0 mL of deionized water was added. With a constant stirring of 360 rpm, the mixture was titrated with excess 1.5 M NaOH at the rate of 5 mL/min until the solution became black. Then, the black particles were filtered and washed with deionized water and ethanol. Finally, the obtained product was dried at room temperature to remove the remaining ethanol.

### **2.3.4. Preparation of Carbon Sphere Based Molecularly Imprinted Chitosan Polymer**

Carbon sphere (CS) based molecularly imprinted chitosan polymer (MICP) was prepared as follow (Ostovan et al. 2018): under magnetic stirring, 0.52 g of chitosan was dissolved in 50.0 mL of (1.0%, v/v) acetic acid solution. After, 0.33 mmol (0.082 g) of pyridoxal phosphate was added to the chitosan solution and allowed to form a pre-complex with chitosan (pyridoxal phosphate-chitosan complex), the mixture was stirred for 2 h. Next, 0.25 g of CS was added and the solution was stirred for a further 24 h vigorously. Then, 50.0 mL 1.0 M NaOH solution was added swiftly into the solution and stirring was continued for 3 h. The obtained product was centrifuged followed rinsed several times with deionized water until the pH of the washing solution was neutral. Afterward, the obtained product was redispersed in 100.0 mL 0.5 M H<sub>2</sub>SO<sub>4</sub> for 5 min in ultrasonic bath. Lastly, MICP was obtained by repeatedly eluting the template (pyridoxal phosphate) with deionized water-methanol (50:50, v/v) until template molecule was entirely eliminated. The non-imprinted polymers (NICP) were prepared by the same procedure without the template molecule.

### **2.3.5. Preparation of Fe<sub>3</sub>O<sub>4</sub> Based Molecularly Imprinted Chitosan Polymer**

Preparation procedure of Fe<sub>3</sub>O<sub>4</sub> based MICP was similar to the procedure mentioned in Section 2.3.3 (Díaz-Hernández et al. 2018). Shortly, in a 500 mL beaker, 100.0 mL of 0.5 M FeCl<sub>3</sub>·6H<sub>2</sub>O solution, 50.0 mL of 0.5 M FeSO<sub>4</sub>·7H<sub>2</sub>O solution and 50.0 mL of chitosan solution were mixed with constant stirring for 1 h. A 0.50 mmol of template molecule (pyridoxal phosphate) was added to the solution and the mixture was stirred for 2 h to form the pre-complex. The mixture was then titrated with excess 1.5 M NaOH at a rate of 5 mL/min with constant stirring at 360 rpm until the solution became black. The particles were then filtered and cleaned with deionized water and ethanol. Finally, the product was allowed to dry at ambient temperature in order to eliminate any residual ethanol. The non-imprinted polymer was prepared by the same procedure without the template molecule.

### **2.4. Synthesis of Inorganic Molecularly Imprinted Polymer by Sol-gel Process**

Inorganic molecularly imprinted polymers were synthesized as follows: 0.50 mmol of pyridoxal phosphate was dissolved in 20.0 mL of deionized water and 50.0 mL of tetrahydrofuran (THF) was added. After stirring for 30 min, 2.0 mL of (3-aminopropyl) triethoxysilane (APTES) was added to the solution and the mixture was stirred for 30 min. Afterward, 3.5 mL of tetraethyl orthosilicate (TEOS) was added to the mixture and stirred for 30 min. Then, 10.0 mL of ethanol and 7.0 mL of NH<sub>3</sub>·H<sub>2</sub>O was added to the mixture and the mixture was stirred vigorously for 24 h. The resultant product was centrifuged and the obtained silica particles was then washed with methanol:acetic acid (90:10, v:v) until the template molecule is removed from the sorbent particles. Non-imprinted silica particles were prepared with the same procedure without the addition of the template molecule.

## 2.5. Characterization Studies

### 2.5.1. Characterization of Chitosan

Sorption performance and solubility properties of chitosan are based on the conditions employed during preparation, such as the treatment temperature, NaOH concentration, and time of reaction. The product may vary from one synthesis batch to the next. Each approach yields a distinct molecular weight and degree of deacetylation, highlighting the physicochemical characterization needs for chitosan.

#### 2.5.1.1. Infrared Spectroscopy

An FTIR spectrometer with an attenuated total reflectance unit was used to record the infrared spectra of dried chitosan and chitin. Table 2.2 shows the characteristic peak locations for each chemical.

Table 2.2. Some functional groups and their IR bands positions. (Source: Solomons and Fryhle 2000)

Functional groups	Frequency range (cm <sup>-1</sup> )
N-H	1100-800
C-O	1050-1300 (strong)
C-N	1180–1360 (strong)
C-H	1340-1470 (strong)
Carbonyl (amide)	1630-1690
C-H	2850-2970 (strong)
O-H	3200-3600 (broad)
N-H	3300-3500 (medium)

## 2.5.1.2. Degree of Deacetylation

### 2.5.1.2.1. Potentiometric Titration

Potentiometric titration was used to determine the degree of deacetylation of chitosan. The method is based on the titration of chitosan with standardized NaOH solution for the deprotonation of the positively charged amine functional groups in chitosan. To accomplish this, 250.0 mg of chitosan was dissolved in 10.0 mL of 0.30 M hydrochloric acid, diluted to 50.0 mL with deionized water, and titrated with 0.100 M NaOH solution. The volume of NaOH consumed, corresponding to the amount of amine groups in chitosan, is derived from the difference between the two inflection points of the acid-base titration (Tolaimate et al. 2000). Degree of acetylation (AD) is calculated by the formula described in Equation 1. The constants 161 and 42 are the molecular weight of glucosamine unit of chitosan and the difference in molecular mass between chitin and chitosan repetitive units, respectively. Molarity of NaOH is  $M$ , volume of NaOH used is  $\Delta V$  and the mass of the chitosan sample used in the analysis is  $m$ . Degree of deacetylation (DD) is calculated by using Equation 2.

$$AD = \left( \frac{1 - 161 \times \frac{\Delta V \times M}{m}}{\frac{\Delta V \times M}{m} \times 42 + 1} \right) \quad (1)$$

$$DD = 1 - AD \quad (2)$$

### 2.5.1.2.2. Elemental Analysis

Elemental analysis, as it is known, reveals the percentage of C, N, H, and S in a material. One oxygen atom and two carbon atoms are removed from the chitin structure during the deacetylation process. The C and O contents of chitosan and chitin structures change, although N remains constant in both forms. As a result, C/N ratios are employed in Equation 3 to calculate the degree of deacetylation (DD) (Kasaai et al. 2000). The ratio

of C/N in totally N-deacetylated chitosan subunit is 5.145, whereas that of N-acetylated chitin subunit is 6.816.

$$DD = \left(1 - \frac{C/N - 5.145}{6.816 - 5.145}\right) \quad (3)$$

## 2.5.2. Characterization of the Sorbents

Various methods were utilized to characterize the sorbents, including potentiometric titration, elemental analysis, scanning electron microscopy (SEM), energy dispersive X-ray (EDX) spectroscopy, thermogravimetric analysis (TGA), and X-Ray diffraction (XRD).

## 2.6. Sorption Studies

### 2.6.1. Binding Characteristic Assay

Rebinding tests were used to determine the binding capacities and dissociation constants of molecularly imprinted and non-imprinted polymers.

Pyridoxal phosphate solutions (10.0 mL) of various concentrations were prepared in ultra-pure water and 10.0 mg of MIP/NIP sorbents were added into each. In a batch equilibration study, the mixtures were shaken at 50 rpm for 24 hours and then filtered using cellulose acetate membrane filters (0.2  $\mu\text{m}$  pore size). The effluents were measured for the detection of pyridoxal phosphate by HPLC-DAD at 297 nm. The procedure was repeated for each sorbent. The experimental parameters are given in Table 2.3. Equation 4 was used to determine the adsorption capacity,  $Q$ .

$$Q = \frac{(C_i - C_f) \times V}{m} \quad (4)$$

$Q$  and  $Q_{max}$  (mmol/g) are the amount of pyridoxal phosphate absorbed at equilibrium and saturation conditions, respectively.  $C_i$  and  $C_f$  (mg/L) are the initial and final pyridoxal phosphate concentrations remained in the solution,  $V$  (L) is the total volume of the sample,  $m$  (g) is the mass of the sorbent.

Table 2.3. Extraction conditions used in binding characteristic assay.

Standard concentrations	1.0, 5.0, 10.0, 25.0, 50.0, 75.0, 100.0 mg.L <sup>-1</sup>
Amount of sorbent	10.0 mg
Sample volume	10.0 mL
Sorption time	24 h
Shaking speed	50 rpm
Ambient temperature	25 °C

## 2.6.2. Selectivity Experiments

To determine whether MIP recognition towards pyridoxal phosphate is selective, MIP/NIP sorption was carried out in the presence of pyridoxamine, nicotinic acid (vitamin B3), pyridoxal and 4-pyridoxic acid (each at 5.0 mg.L<sup>-1</sup>) while maintaining the other parameters constant (10.0 mL sample volume, 10.0 mg MIP/NIP sorbent, 24 hours shaking time at 50 rpm).

In addition to the selectivity experiment mentioned before, the distribution coefficients of the analytes,  $K_d$  (mg g<sup>-1</sup>), were calculated using Equation 5, in which  $C_0$  stands for the initial concentration of analyte (mmol.L<sup>-1</sup>) before sorption, and the final concentration of the analyte remaining in the liquid phase after sorption is indicated as  $C_e$  (mmol.L<sup>-1</sup>). The solution volume (mL) and the weight of the polymer (g) are shown as  $V$  and  $W$ , respectively. By using Equation 6, in the presence of competing compounds, the selectivity coefficient for sorption of pyridoxal phosphate ( $K$ ) was calculated. Finally, to check the selectivity of MIP/NIP, the relative selectivity coefficient ( $K'$ ) was determined by using Equation 7 (Boyacı et al. 2010).

$$K_d = \frac{C_0 - C_e}{WC_e} V \quad (5)$$

$$K = \frac{K_d(\text{pyridoxal phosphate})}{K_d(\text{competitor analyte})} \quad (6)$$

$$K' = \frac{K(\text{MIP})}{K(\text{NIP})} \quad (7)$$

### 2.6.3. Effect of Sorption Time on the Extracted Amount of the Analyte

To obtain the optimum sorption time, 10.0 mL of 5.0 mg.L<sup>-1</sup> of pyridoxal phosphate standard solutions in ultra-pure water were used. 10.0 mg sorbents were weighed in vials and 10.0 mL of the standard solutions were added into each. The mixtures were shaken at 50 rpm and then filtered with cellulose acetate membrane filter (0.22 µm pore size) prior to the HPLC-DAD analysis of effluents at 297 nm. The experimental parameters for the investigation of sorption time is given in Table 2.4.

Table 2.4. Experimental parameters employed for the investigation of the effect of sorption time on the sorption pyridoxal phosphate.

Standard concentration	5.0 mg.L <sup>-1</sup>
Sorbent amount	10.0 mg
Sample solution volume	10.0 mL
Shaking times	5, 15, 30, 60, 120, 240, 480, 720, 1440 min

### 2.6.4. Effect of Sorbent Amount on the Extracted Amount of Analyte

The sorbents were weighed in vials at different amounts as shown in Table 2.5. in order to evaluate the influence of sorbent quantity on pyridoxal phosphate sorption. For this purpose, 10.0 mL of 5.0 mg.L<sup>-1</sup> of pyridoxal phosphate standard solutions were prepared in ultra-pure water, added to each vial and mixed at 50 rpm for 24 h. Afterward, the samples were filtered using cellulose acetate membrane filter (0.22 µm pore size). Finally, the effluents were analyzed by using HPLC-DAD at 297 nm.

Table 2.5. Experimental parameters to analyze the effect of sorbent amount for sorption of pyridoxal phosphate.

Standard concentration	5.0 mg.L <sup>-1</sup>
Sorbent amount	0.5, 1.0, 3.0, 5.0, 10.0 mg
Sample solution volume	10.0 mL
Sorption time	24 h

### 2.6.5. Effect of Sample Volumes

To test the influence of sample volume on sorption, 10.0 mg sorbents were weighed into vials. The vials with sorbents were then added with various volumes of 5.0 mg.L<sup>-1</sup> pyridoxal phosphate solution, as shown in Table 2.6, the vials were shaken at 50 rpm for 24 hours and at the end of the period, were filtered through using 0.2 µm pore size cellulose acetate membranes. The results were evaluated after the analysis using HPLC-DAD at 297 nm.

Table 2.6. Experimental parameters used for the investigation of the effect of sample volume on the sorption of pyridoxal phosphate

Standard concentration	5.0 mg.L <sup>-1</sup>
Sorbent amount	10.0 mg
Solution volumes	1.0, 3.0, 5.0, 10.0, 20.0 mL
Sorption time	24 h

### 2.7. Sorption Isotherm models

An isotherm is a curve that describes the retention of a molecule on a solid at different concentrations and is used to forecast the molecule's migration in the environment (Limousin et al. 2007).

Langmuir adsorption isotherm considers that the adsorption energy is constant and that adsorption happens at a specific number of definite localized homogeneous sites (limited number of binding sides) with monolayer adsorption (Gueu et al. 2007; Limousin et al. 2007; Qi and Xu 2004).

Equation 8 gives the Langmuir nonlinear form;

$$Q_e = Q_{max} \frac{bC_e}{1+bC_e} \quad (8)$$

at which  $Q_{max}$  (mmol.g<sup>-1</sup>) and  $b$  (L.mmol<sup>-1</sup>) are Langmuir constants,  $Q_{max}$  is the amount of pyridoxal phosphate adsorption relating to monolayer coverage,  $b$  is the affinity of pyridoxal phosphate for the sorbent,  $C_e$  (mmol.L<sup>-1</sup>) is the amount of pyridoxal phosphate in liquid phase at equilibrium, and  $Q_e$  (mmol.g<sup>-1</sup>) is the quantity of pyridoxal phosphate deposited on the surface of the sorbent at equilibrium. The constant values are calculated using the linearized version of Equation 8 which is given in Equation 9.

$$\frac{1}{Q_e} = \frac{1}{Q_{max}} + \frac{1}{Q_{max}bC_e} \quad (9)$$

The values of  $Q_{max}$  and  $b$  are determined using the intercept and slope of the  $1/Q_e$  versus  $1/C_e$  plot.

Freundlich described an isotherm for heterogeneous surfaces, with the constraint of small concentrations. As the saturation point approaches, the isotherm deviates (Umpleby et al. 2001).

The nonlinear isotherm by Freundlich is given in Equation 10.

$$Q_e = K_F C_e^{1/n} \quad (10)$$

at which, for this particular sorbent-adsorbate system,  $K_F$  and  $n$  are constants. In Equation 11, these constant can be calculated from the linearized form of the equation.

$$\log Q_e = \log K_F + \frac{1}{n} \log C_e \quad (11)$$

$K_F$  and  $1/n$  are calculated from the intercept and the slope of the  $\log Q_e$  versus  $\log C_e$  equation plot, respectively.

The Dubinin-Radushkevich (D-R) isotherm model claims that ionic species selectively attach to the most energetically favorable sites of the sorbent associated with ion multilayer adsorption (Guibal, Milot, and Tobin 1998). The D-R isotherm is usually defined in the Equation 12 (Kavitha and Namasivayam 2007);

$$Q_e = q_s e^{(-B\varepsilon^2)} \quad (12)$$

where;

$$\varepsilon = RT \ln \left( 1 + \frac{1}{C_e} \right) \quad (13)$$

The Dubinin-Radushkevich parameter,  $q_s$ , relates to the sorption monolayer capacity and B, gives the mean free energy of adsorption per adsorbate molecule needed for transit to the solid's surface from infinity in the solution (Şeker et al. 2008). By using Equation 14, the mean free energy of the sorption can be calculated from the D-R parameter B.

$$E = \sqrt{(2B)} \quad (14)$$

$q_s$  and B constants are obtained from the slopes and the intercepts of experimental plots of  $\ln q$  versus  $\varepsilon^2$ .

The Harkins-Jura model is applicable to multilayer adsorption and may be explained by the presence of heterogeneous pore distribution. The constant A accounts for multilayer adsorption and explains the presence of heterogeneous pore distribution and the constant B is the isotherm constant in H-J equation (Erdogan 2019). The H-J isotherm is defined in Equation 15.

$$\frac{1}{q_e^2} = \left( \frac{B}{A} \right) - \left( \frac{1}{A} \right) \log C_e \quad (15)$$

The Chi-Square test is a statistical tool used to compare observed and anticipated data. This test may also be performed to see if it corresponds with our data's categorical variables. It aids in determining if a discrepancy between two category variables is the result of chance or of a link between them. It is represented by the sign  $X^2$ . The observed adsorption capacity is  $Q_{experimental}$ , whereas the predicted adsorption capacity is  $Q_{model}$ . The Chi-Square fit test value is obtained using the formula in Equation 16.

$$X^2 = \sum \frac{(Q_{experimental} - Q_{model})^2}{Q_{model}} \quad (16)$$

For 1.0, 5.0, 10.0, 25.0, 50.0, 75.0, and 100.0 mg/L of pyridoxal phosphate concentrations, isotherm models for pyridoxal phosphate sorption by the sorbents were examined. The solution volume, shaking duration, sorbent amount, and ambient temperature were 10.0 mL, 24 hours, 10.0 mg, and 25°C, respectively.

## 2.8. Desorption Studies

Table 2.7. Experimental parameters used for the investigation of the effect of eluent type on the elution of pyridoxal phosphate.

Standard concentration	5.0 mg.L <sup>-1</sup>
Sorbent amount	10.0 mg
Sample volume	10.0 mL
Sorption time	24 h
Eluents	PBS buffer (pH: 7.6) Mobile phase NaOH (2%) : NaCl (3%) Acetic acid (2%, v/v) Acetic acid (4%, v/v) Acetic acid (6%, v/v)
Eluent volume	10.0 mL
Desorption time	24 h

Various solutions were tested in order to determine the optimal eluent that is capable of quantitatively desorbing pyridoxal phosphate from the sorbents. In a typical procedure, 10.0 mL of 5.0 mg.L<sup>-1</sup> pyridoxal phosphate was added to a vial containing 10.0 mg of MICP (or MMICP or IMIP). The vials were shaken at 50 rpm. After the sorption step, the sorbents were separated from the solutions and desorption of pyridoxal phosphate was done using the eluents listed in Table 2.7. The sorbent was then removed from the elution solution by filtration, and the eluent was evaluated using HPLC-DAD.

## 2.9. Method Validation

Water samples (distilled, bottled, and tap water) and two types of artificial serum samples were spiked with standard pyridoxal phosphate solution. The ability of the sorbents to absorb pyridoxal phosphate in various types of matrices was studied. The concentration of pyridoxal phosphate, sample volume, shaking time, sorbent amount and sorption temperature were 5.0 mg.L<sup>-1</sup>, 10.0 mL, 30 min, 10.0 mg and 25 °C, respectively. After filtration, the eluents were employed to desorb pyridoxal phosphate from the sorbents. The desorption conditions mentioned in Section 2.8 were employed in the study.

Two different synthetic serum formulations were prepared and tested as samples. The first serum (formulation 1) was prepared according to the procedure in (Uygun and Sezgintürk 2011), and consisted of 4.5 mM KCl, 5 mM CaCl<sub>2</sub>, 1.6 mM MgCl<sub>2</sub>, 4.7 mM d(+)-glucose, 2.5 mM urea, 0.1% BSA, and 145 mM NaCl, which was spiked with pyridoxal phosphate as necessary. The second serum solution (formulation 2) was created by adding BSA to phosphate buffered saline (PBS) to obtain 6% (m:v) BSA in final solution. pH of this solution was pH 7.6. It is known that most of the PLP is bound to albumin (Fonda et al. 1991). Therefore, a sample pre-treatment procedure that converts the protein-bound form of the analyte to its free form before the MIP-SPE stage must be used to achieve high recoveries. Several protein precipitation approaches have been documented that can be used on a biological matrix containing proteins. The precipitation of the proteins increases the free concentration of the analytes and prevents potential interference effect of macromolecules. For this purpose, organic solvents are often chosen in the protein precipitation process (Jiménez et al. 1988) due to their ease of use. Therefore, in this research, a 50:50 (v:v) methanol-water solution was employed to precipitate BSA from synthetic serum samples, leaving the analytes free in the sample.

## CHAPTER 3

### RESULTS AND DISCUSSIONS

#### 3.1. Optimization of Instrumental Parameters

During the study, the instrumental parameters listed in Table 2.1 were used. Waters Spherisorb ODS2 (5  $\mu\text{m}$  4.6x250 mm) column was utilized for chromatographic separation under isocratic run conditions with 1.0 mL.min<sup>-1</sup> flowrate of the mobile phase MeOH:H<sub>2</sub>O (5:95, H<sub>2</sub>O contains 0.2% (v/v) TFA), temperature of 30°C, sample injection volume of 20.0  $\mu\text{L}$ . These conditions were employed in all relevant tests throughout the study unless stated otherwise. Chromatogram of pyridoxamine, nicotinic acid (vitamin B3), pyridoxal, pyridoxal phosphate and 4-pyridoxic acid is given in Figure 3.1. Figure 3.2 demonstrates the calibration plots of pyridoxamine, nicotinic acid (vitamin B3), pyridoxal, pyridoxal phosphate and 4-pyridoxic acid. The equations of the calibration curves, R<sup>2</sup> values and calculated LOD and LOQ values are given in Table 3.1.

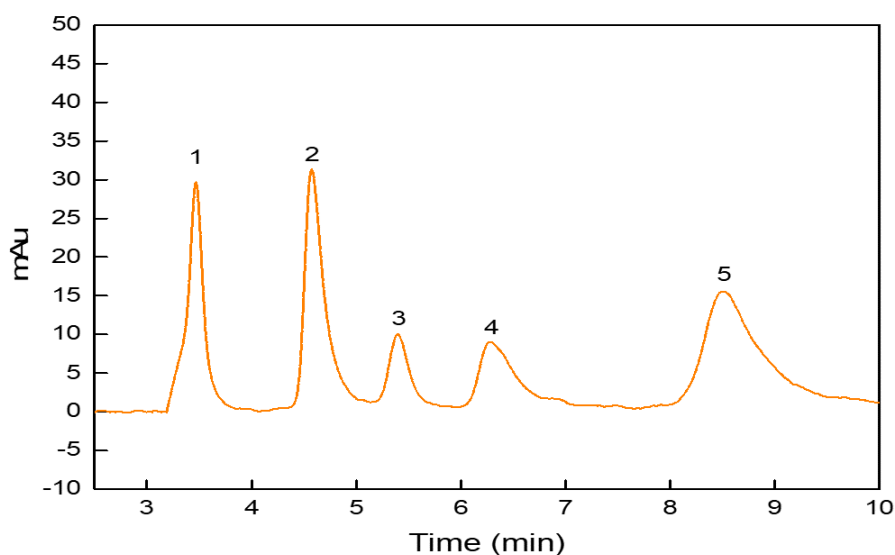


Figure 3.1. Chromatogram of standard solution containing (1) pyridoxamine, (2) nicotinic acid (vitamin B3), (3) pyridoxal, (4) pyridoxal phosphate and (5) 4-pyridoxic acid.

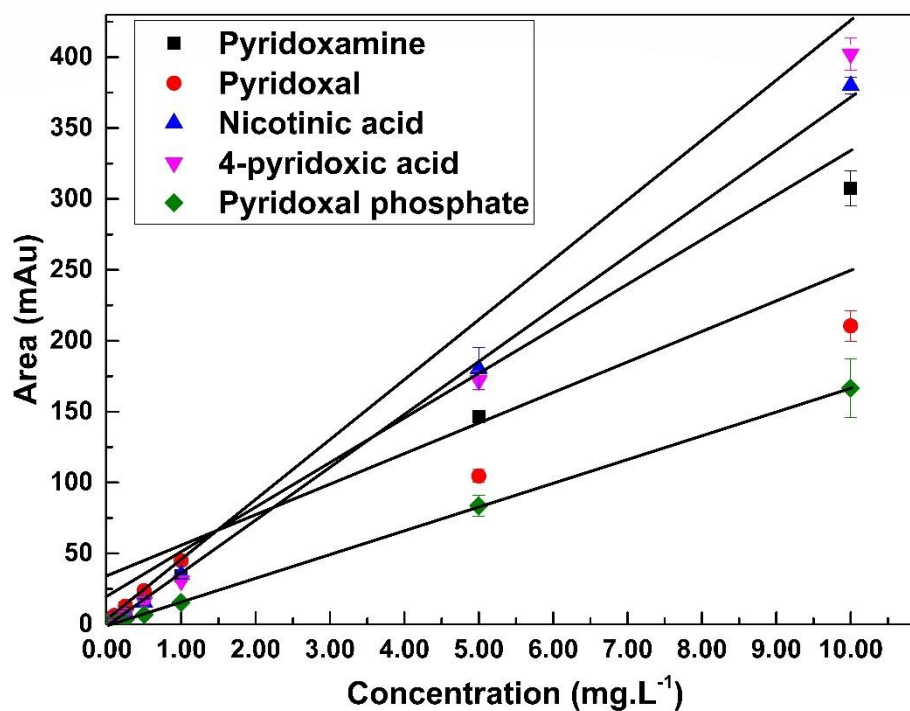


Figure 3.2. Calibration plots for pyridoxamine, pyridoxal, nicotinic acid, 4-pyridoxic acid and pyridoxal phosphate.

Table 3.1. The line equations of the calibration curves,  $R^2$  values and calculated LOD and LOQ values.

Analyte	LOD ( $\text{mg.L}^{-1}$ )	LOQ ( $\text{mg.L}^{-1}$ )	Equation	$R^2$
Pyridoxamine	0.13	0.40	$y = 30.323x + 1.3312$	0.9992
Pyridoxal	0.58	1.76	$y = 20.186x + 8.1608$	0.9983
Nicotinic acid	0.12	0.38	$y = 37.861x - 2.156$	0.9995
4-pyridoxic acid	0.36	1.10	$y = 39.595x - 4.583$	0.9954
Pyridoxal phosphate	0.06	0.18	$y = 16.701x - 0.3785$	0.9999

## 3.2 Sorbent Characterization Studies

### 3.2.1 Characterization of Chitosan

#### 3.2.1.1 Infrared Spectroscopy

FT-IR was used to check the presence of related functional groups of chitosan obtained by the deacetylation of chitin. When the deacetylation of chitin occurs, the carbonyl peak of amide at  $1630\text{--}1660\text{ cm}^{-1}$  disappears indicating the formation of chitosan (Figure 3.3). For comparison, the spectrum of commercial chitosan was also obtained. Because the structures of chitin and chitosan (seen in Fig 2.1) are related, the closely related peaks can be seen in the spectra; N-H peak at about  $1050\text{ cm}^{-1}$ ,  $1200\text{--}1600\text{ cm}^{-1}$  and around  $2900\text{ cm}^{-1}$ , C-O at around  $1200\text{ cm}^{-1}$ , C-N at  $1200\text{--}1600\text{ cm}^{-1}$  and O-H at  $3000\text{--}3600\text{ cm}^{-1}$ .

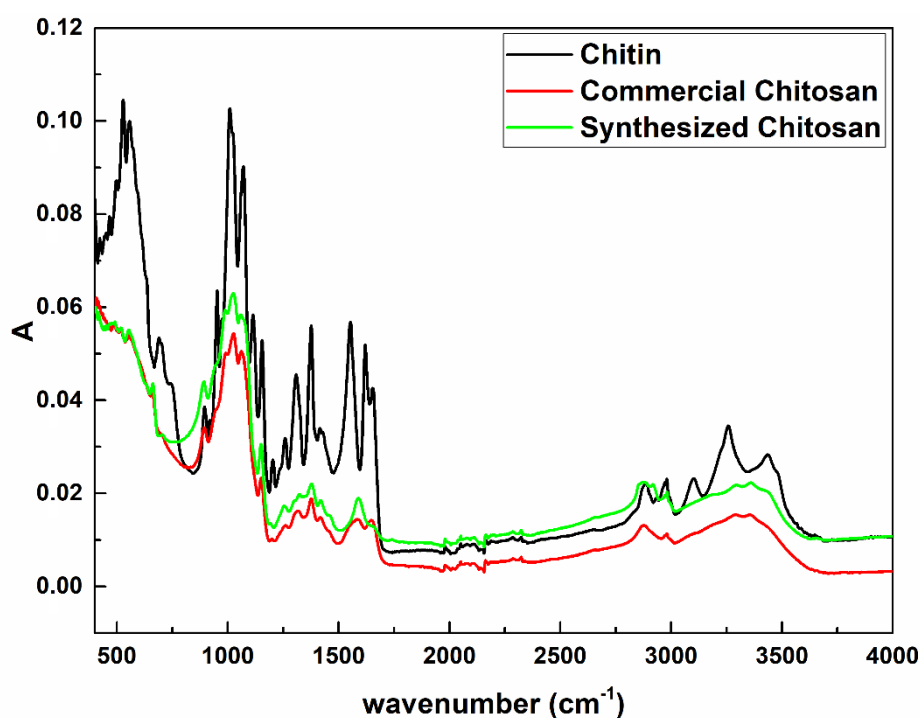


Figure 3.3. FT-IR spectra of chitin and chitosan.

#### 3.2.1.2 Degree of Deacetylation of Synthesized Chitosan

Degree of deacetylation of chitosan was determined using the procedures outlined in Section 2.5.1.2. Figure 3.4 displays the potentiometric titration graph of chitosan

dissolved in HCl. The difference between the two inflection points corresponds to the quantity of protonated amine groups in chitosan. The titrimetric approach for determining the degree of deacetylation yielded a 95.3 percent elimination of acetyl groups, which agreed with the result of elemental analysis. The results of the elemental analysis by EDX for synthesized chitosan are demonstrated in Table 3.2. The degrees of deacetylation determined by the stated procedures are shown in Table 3.3 for comparison.

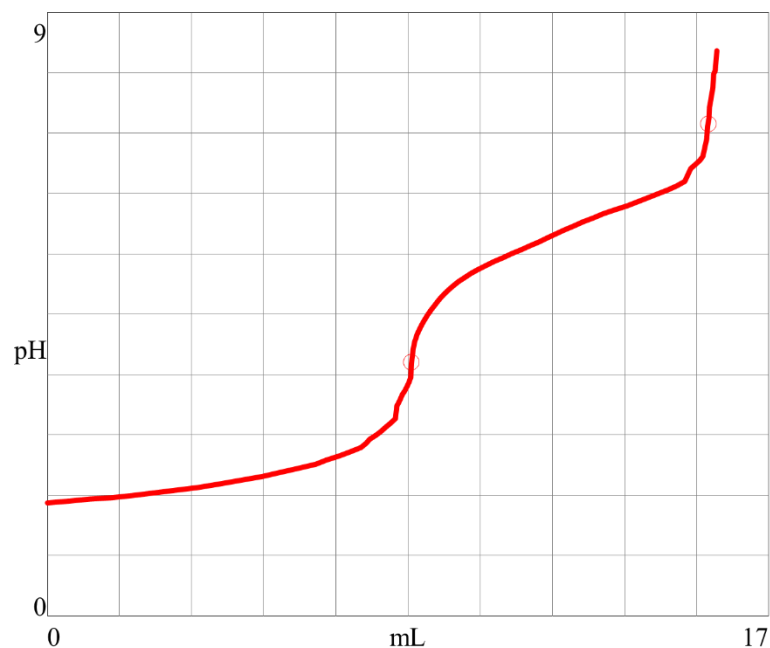


Figure 3.4. Potentiometric titration of synthesized chitosan with standardized NaOH solution.

Table 3.2. Elemental analysis of synthesized chitosan by EDX.

Compound	C%	N%	O%
Synthesized chitosan	59.39	11.33	27.68

Table 3.3. Degree of deacetylation of chitosan by two methods.

Method	D.A %	D.D%
Potentiometric titration	4.7	95.3
Elemental analysis	5.8	94.2

### 3.2.2 Morphological Characterization of Carbon Sphere

Scanning electron microscopy (SEM) was used for the examination of the morphology of carbon sphere. Carbon sphere particles were placed onto SEM planchets and all samples were coated with gold before getting images. Figure 3.5 shows the SEM images of carbon spheres.

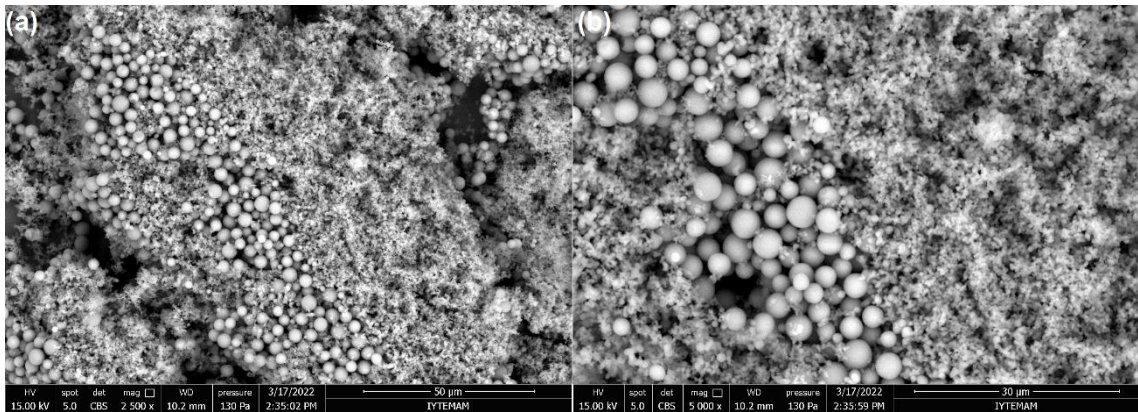


Figure 3.5. SEM images of carbon sphere (magnification by: (a) 2500x times and (b) 5000x times.

### 3.2.3 Morphological Characterization of Fe<sub>3</sub>O<sub>4</sub> Nanoparticles

The SEM micrographs of pure Fe<sub>3</sub>O<sub>4</sub> nanoparticles (Figure 3.6 (a) and (b)) are shown. Observing the photographs, nanoparticles were aggregated seriously, which was due to the nanosized of the Fe<sub>3</sub>O<sub>4</sub>.

The EDX spectrum of Fe<sub>3</sub>O<sub>4</sub> nanoparticles is shown in Figure 3.7. The elemental composition of the material, as indicated in Table 3.4, suggests that it is mostly made of Fe, and O. The spectrum, however, contains Na signal, which most likely reflect the precipitation of sodium chloride generated during the production of the nanoparticle material from the chemical precursors.

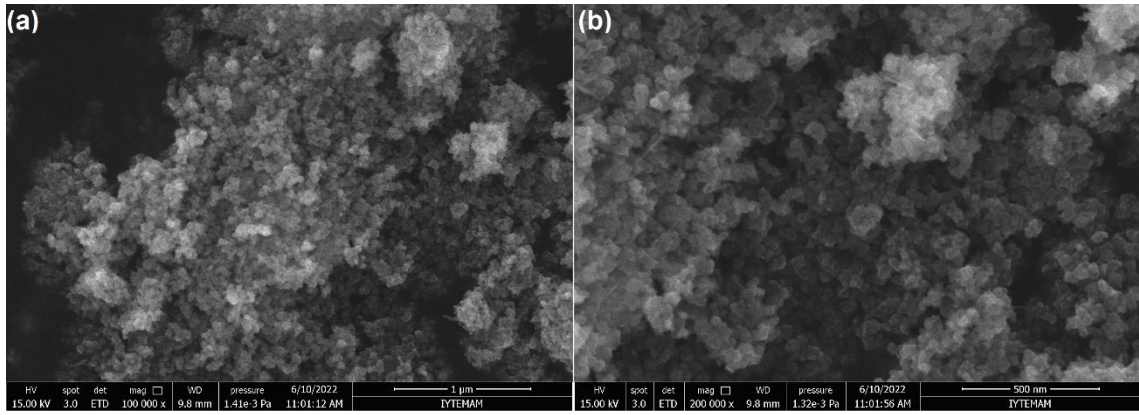


Figure 3.6. SEM images of Fe<sub>3</sub>O<sub>4</sub> nanoparticles (magnification by: (a) 100000 times and (b) 200000 times).

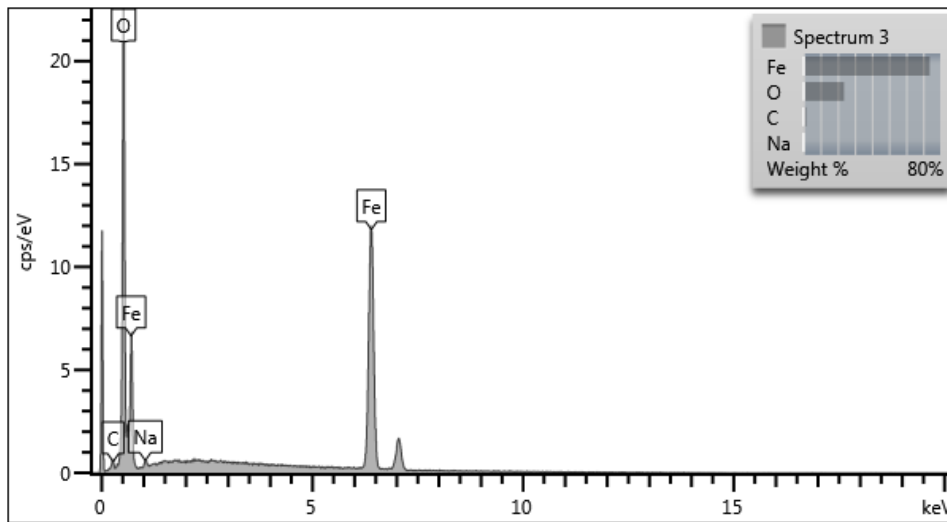


Figure 3.7. EDX graph of Fe<sub>3</sub>O<sub>4</sub> nanoparticles.

Table 3.4. The elemental composition of Fe<sub>3</sub>O<sub>4</sub> nanoparticles analyzed by EDX.

Element	Wt %	Atomic %
C	1.79	4.98
O	23.79	49.84
Na	0.60	0.88
Fe	73.82	44.30
Total	100.00	100.00

The structural characteristics of nanoparticles were investigated using powder X-ray diffraction. Figure 3.8 displays the X-ray diffraction patterns for  $\text{Fe}_3\text{O}_4$  nanoparticles, both alone and in chitosan. The six distinct peaks for  $\text{Fe}_3\text{O}_4$  can be seen at 2 theta values corresponding to  $\text{Fe}_3\text{O}_4$  nanoparticles alone. The decrease in the peak intensities must be due to the dilution of  $\text{Fe}_3\text{O}_4$  by chitosan.

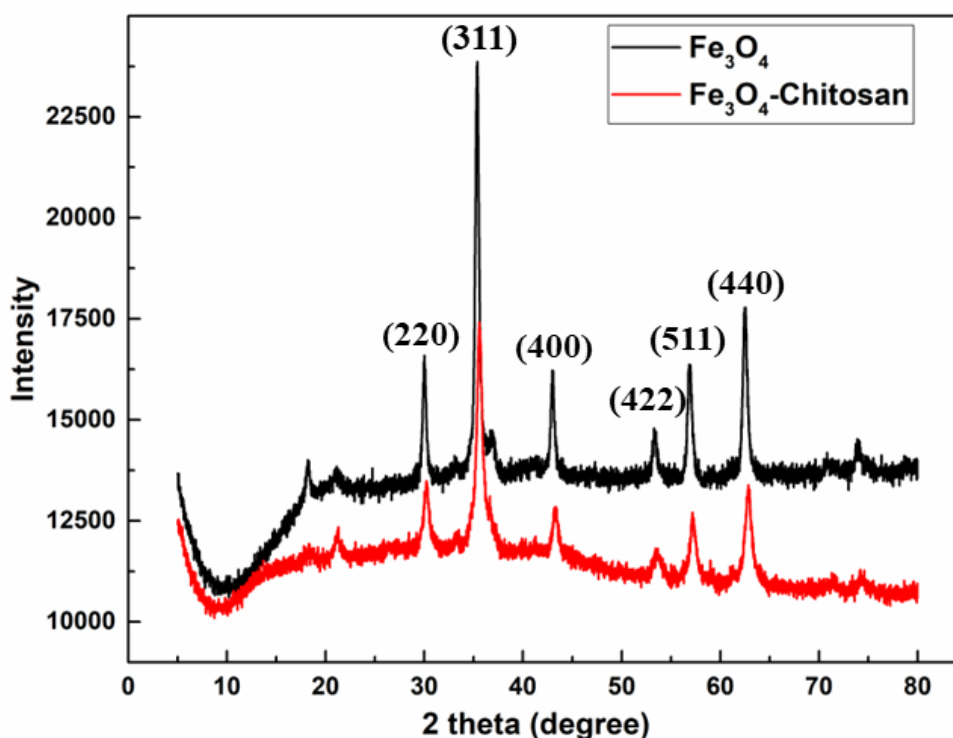


Figure 3.8. X-ray diffraction patterns for  $\text{Fe}_3\text{O}_4$  nanoparticles and  $\text{Fe}_3\text{O}_4$  based molecularly imprinted chitosan polymer (MMICP).

### 3.2.4 Characterization of Carbon Sphere Based Molecularly Imprinted Chitosan Polymer

The morphology of carbon sphere based MICP and NICP was examined using SEM. MICP and NICP particles were deposited on SEM plachets and the samples were coated with gold before the images were taken. The SEM images of the material is seen in Figure 3.9. SEM pictures are thought to be useful tools for identifying form and surface morphology. As seen in the figures, the surface of the material can be said to have a homogeneous distribution of the carbon sphere particles all over the composite structure.

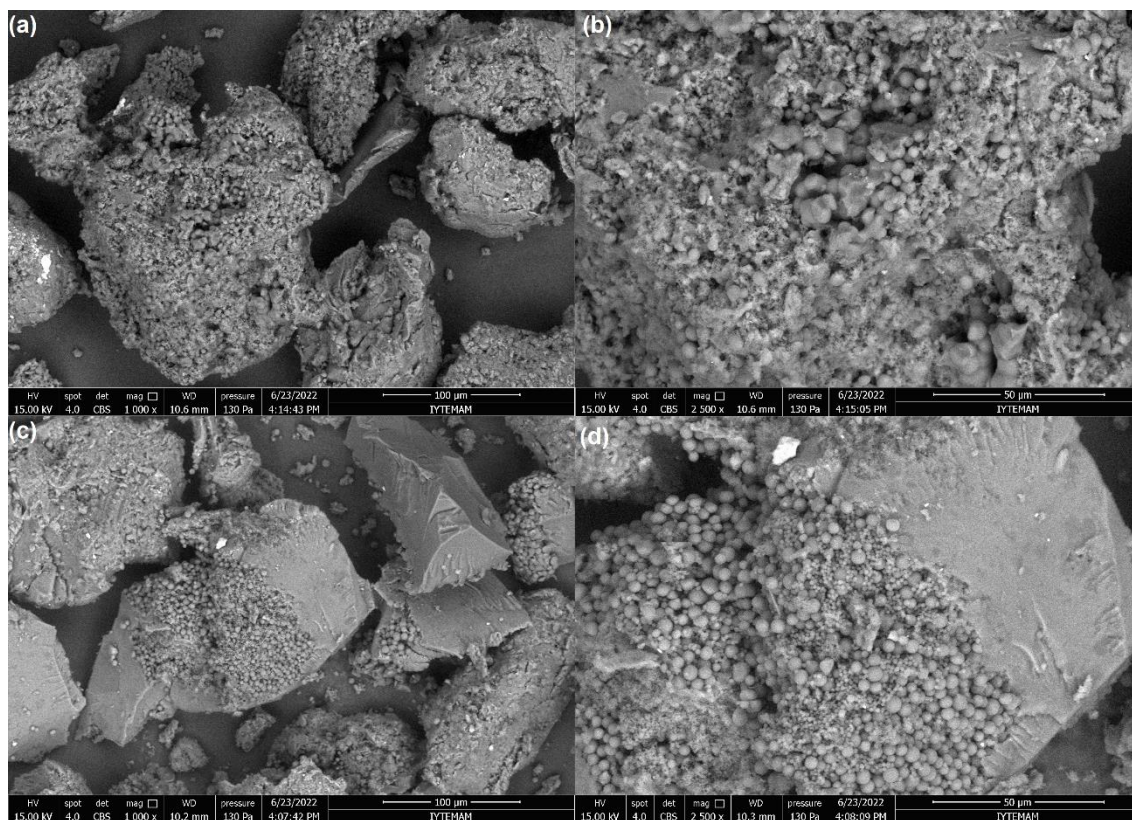


Figure 3.9. SEM images of carbon sphere based molecularly imprinted chitosan polymer (MICP) (a and b) and non-imprinted chitosan polymers NICP (c and d); (a) magnified 1000 times, (b) magnified 2500 times, (c) magnified 1000 times and (d) magnified 2500 times.

### 3.2.5 Characterization of Fe<sub>3</sub>O<sub>4</sub> Based Molecularly Imprinted Chitosan Polymer

The SEM micrographs of Fe<sub>3</sub>O<sub>4</sub> based molecularly imprinted chitosan polymer (Figure 3.10 (a) and (b)) are shown. The sample was placed on the SEM planchets coated with gold before the photographs were shot. From the images, it can be seen that the magnetite particles coated with chitosan homogeneously.

Figure 3.11 displays the EDX spectrum of magnetite based MMICP/MNICP. The spectrum depicts the material's elemental composition. Peaks showing the presence of Fe, C, and O are found, as predicted. Table 3.5 shows the weight and atom percentages of the particles.

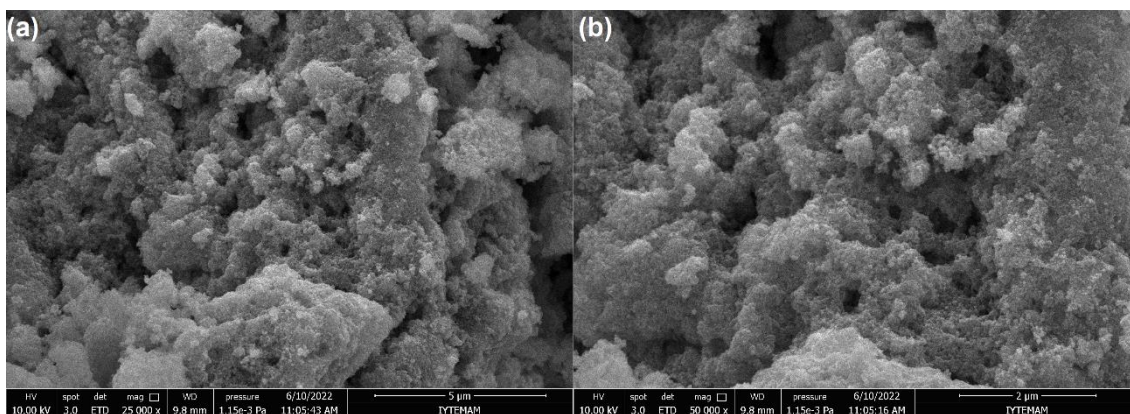


Figure 3.10. SEM images of  $\text{Fe}_3\text{O}_4$  based molecularly imprinted chitosan polymer (MMICP): (a) magnified 25000 times and (b) magnified 50000 times.

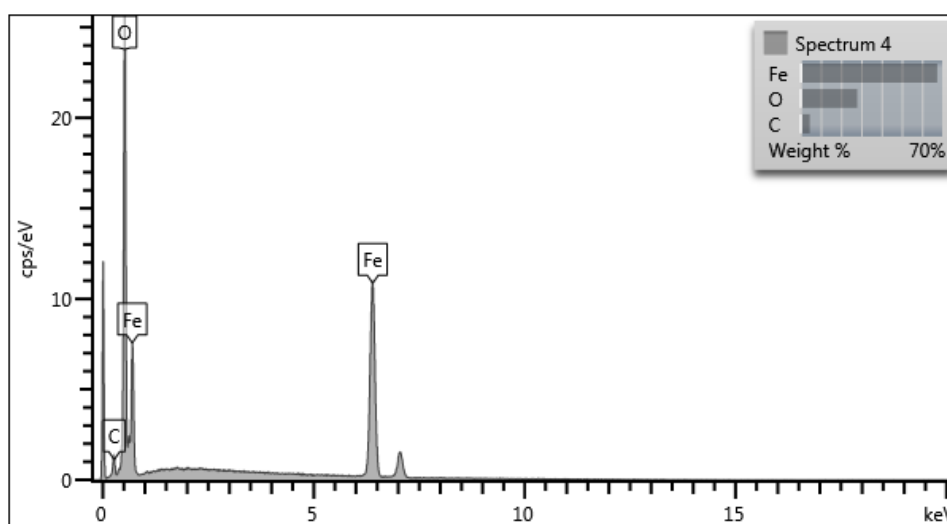


Figure 3.11. EDX graph of  $\text{Fe}_3\text{O}_4$  based molecularly imprinted chitosan polymer (MMICP).

Table 3.5. The elemental composition  $\text{Fe}_3\text{O}_4$  based molecularly imprinted chitosan polymer analyzed by EDX.

Element	Wt %	Atomic %
C	4.53	11.32
O	27.96	52.42
Fe	67.51	36.26
Total	100.00	100.00

Powder X-ray diffraction (XRD) was used to investigate the structural properties of  $\text{Fe}_3\text{O}_4$  based molecularly imprinted chitosan polymer (MMICP) (Figure 3.8). For  $\text{Fe}_3\text{O}_4$  nanoparticles, the six unique peaks are positioned at 2 theta. In comparison, the peak intensities of MMICP is lower than the peak intensities of  $\text{Fe}_3\text{O}_4$  (Figure 3.8). It can be assumed that these intensity decreases are resulted from the chitosan bound to  $\text{Fe}_3\text{O}_4$ .

Thermal gravimetric analyses (TGA) of chitosan,  $\text{Fe}_3\text{O}_4$  nanoparticles and  $\text{Fe}_3\text{O}_4$  based molecularly imprinted chitosan polymer (MMICP) were performed in a temperature range of 25-800 °C. The results of this analysis are shown in Figure 3.12. As can be followed from the figure, the TGA of chitosan showed weight loss in two stages. The first stage ranges between 25-280 °C with 6% weight loss, mainly due to absorbed and adsorbed water loss. The second stage of weight loss starts after 280 °C. This stage corresponds to the degradation of chitosan. As seen in Figure 3.12, chitosan loses weight dramatically after 280 °C. On the other hand,  $\text{Fe}_3\text{O}_4$  based chitosan MIP loses a smaller mass compared to chitosan. Finally, the difference between  $\text{Fe}_3\text{O}_4$  and  $\text{Fe}_3\text{O}_4$  based chitosan MIP shows the loss of chitosan. This weight loss was obtained as 5.7% of the total loss. Based on the added chitosan in the reaction mixture, 8.0% of chitosan is expected to be present in  $\text{Fe}_3\text{O}_4$  based chitosan MIP. Considering that approximately 70% of total loss was observed for chitosan, the 5.7% loss from  $\text{Fe}_3\text{O}_4$  based chitosan MIP indicates that the loss is due to the present chitosan in the structure.

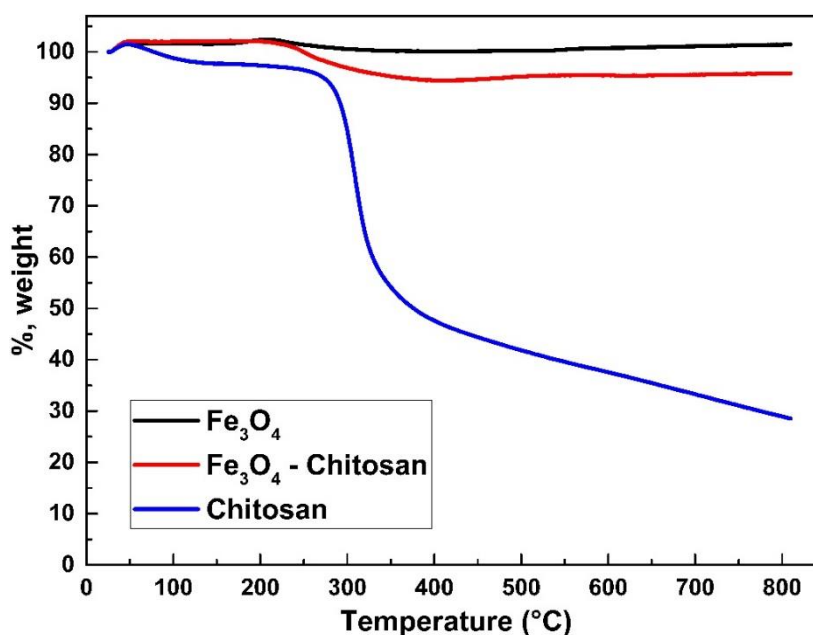


Figure 3.12. TGA thermogram of chitosan,  $\text{Fe}_3\text{O}_4$  nanoparticles and  $\text{Fe}_3\text{O}_4$  based molecularly imprinted chitosan polymer.

### 3.2.6 Characterization Sol-Gel Based Molecularly Imprinted Polymer

Silica (sol-gel) based IMIP and INIP were placed onto SEM plachets and were coated with gold before getting the images. As seen in Figure 3.13 (a and b), the spherical particles of IMIP appear to be distributed homogeneously and exhibit a very smooth surface, while different morphologies are observed at the surface of INIP (Fig. 3.13 c and d).

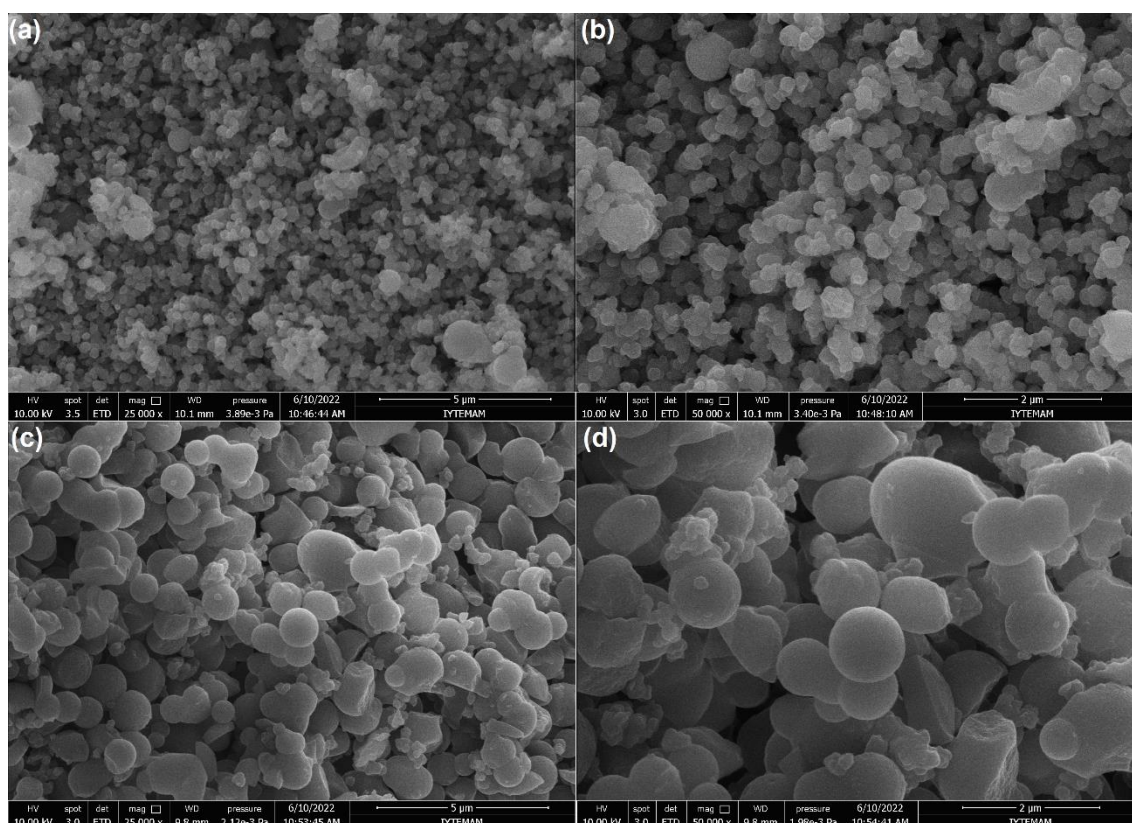


Figure 3.13. SEM images of (a and b) silica (sol-gel) based molecularly imprinted polymers and (c and d) non-imprinted polymers: (a) magnified 25000 times, (b) magnified 50000 times, (c) magnified 25000 times and (d) magnified 50000 times.

Figure 3.14 displays the EDX spectrum of sol-gel based IMIP/INIP. The spectrum demonstrates the material's elemental composition. Peaks showing the presence of Si, C, N and O are found, as predicted. Table 3.6 shows the weight and atom percentages of the silica particles.

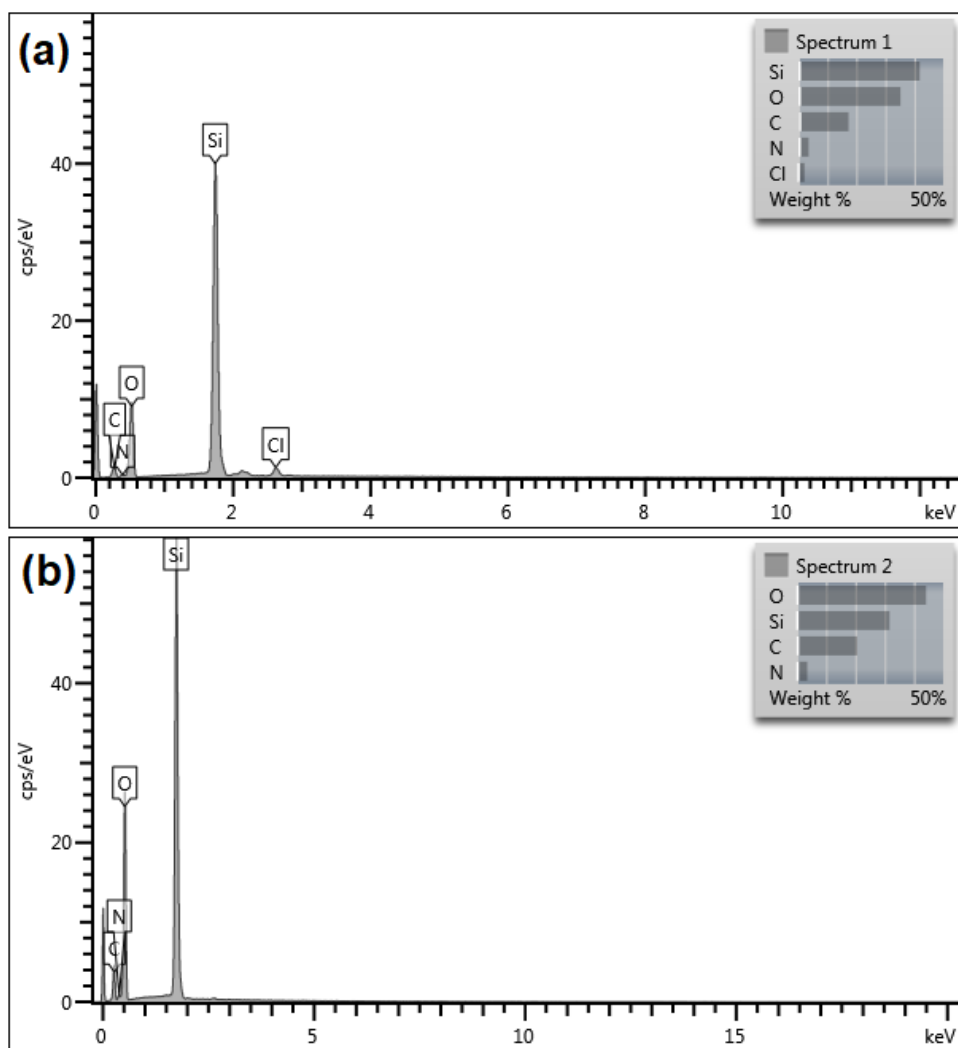


Figure 3.14. EDX graphs of (a) silica (sol-gel) based molecularly imprinted polymer and (b) non-imprinted polymer.

Table 3.6. Elemental compositions of silica (sol-gel) based molecularly imprinted polymer (IMIP) and non-imprinted polymer (INIP).

Element	IMIP		INIP	
	Wt %	Atomic %	Wt %	Atomic %
C	17.33	26.50	20.60	29.27
N	3.54	4.64	3.59	4.37
O	35.22	40.43	44.17	47.13
Si	41.85	27.37	31.64	19.23
Cl	2.06	1.07	0	0
Total	100.00	100.00	100.00	100.00

### 3.3 Sorption Studies

#### 3.3.1 Binding Characteristic Assay

After the preparation/synthesis of carbon sphere based molecularly imprinted chitosan polymer as explained in Section 2.3.4, the sorption performance of the materials was investigated starting from the binding characteristic assay (this is a method to find out whether the MIP after template removal is capable of retention of the analyte). Figure 3.15 displays the sorption capabilities of carbon sphere MICP and NICP as a function of pyridoxal phosphate concentration. The ordinate  $Q$  represents the mmol of pyridoxal phosphate adsorbed by 10.0 g of carbon sphere based MICP or NICP. MICP and NICP demonstrate no meaningful difference at low concentrations. This observation can be ascribed to the ability of even the non-selective functional groups which are present in both MICP and NICP to uptake pyridoxal phosphate at low concentrations. However, when concentration of the analyte increases, the difference in sorption capacities between MICP and NICP grows in favor of MICP; at least up to  $100.0 \text{ mg.L}^{-1}$ .

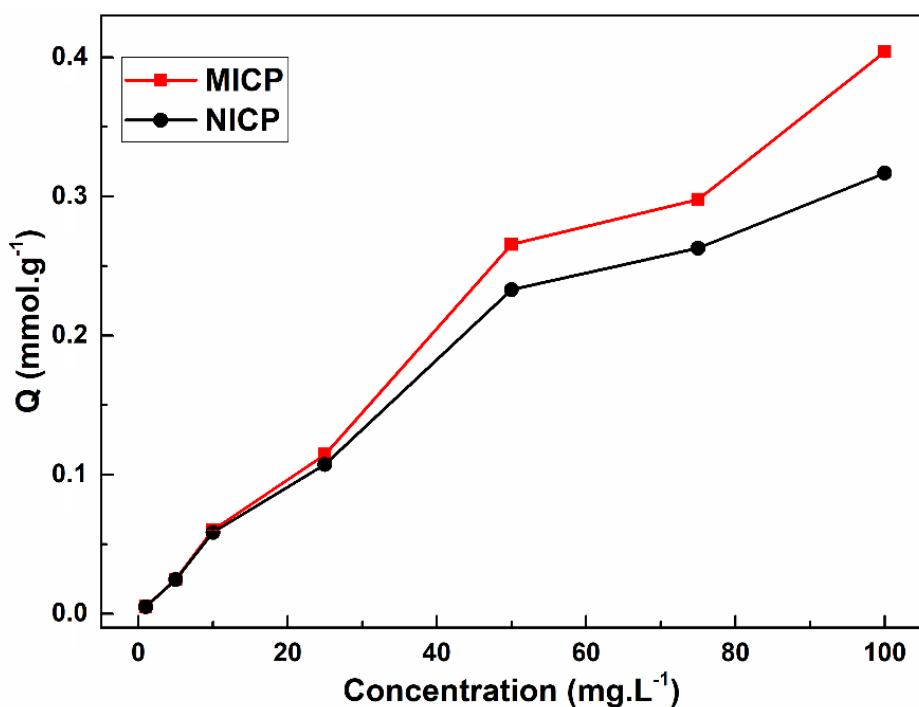


Figure 3.15. Sorption capacities of carbon sphere based MICP and NICP.

The sorption capabilities of Fe<sub>3</sub>O<sub>4</sub> based MMICP and MNICP are shown in Figure 3.16. as a function of pyridoxal phosphate concentration. Similar to the carbon sphere

case, at low concentrations, there is no discernible difference between MMICP and MNICP. However, when the analyte concentration increases, the sorption capacities of MMICP and MNICP differ.

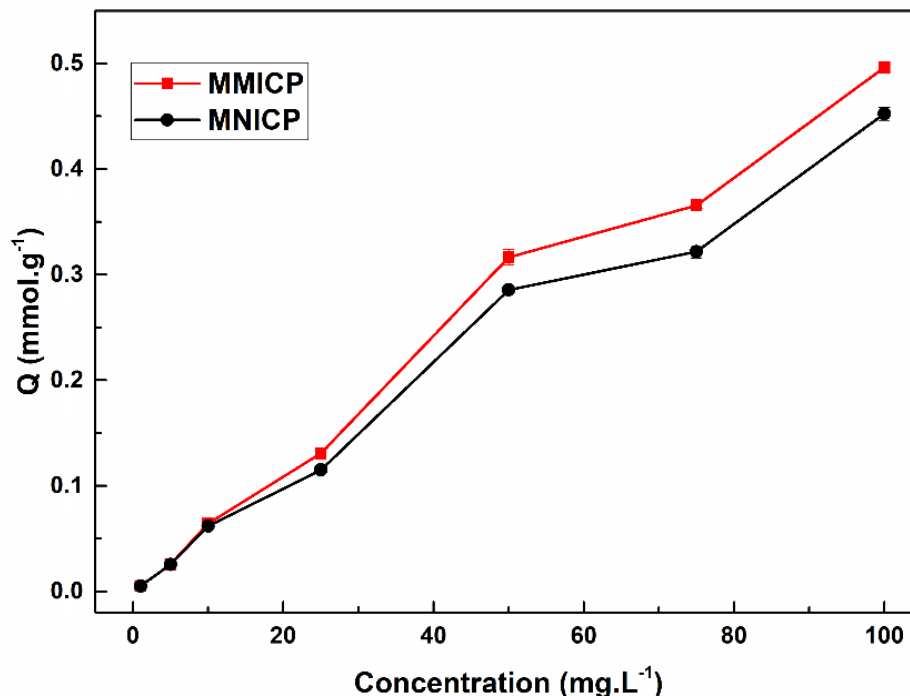


Figure 3.16. Sorption capacities of Fe<sub>3</sub>O<sub>4</sub> based MMICP and MNICP.

The sorption capabilities of silica (sol-gel) based IMIP and INIP are demonstrated in Figure 3.17. as a function of pyridoxal phosphate concentration. As seen in the figure, the sorption capability of IMIP and INIP were better than those of MICP/NICP and MMICP/MNICP couples. However, there is no significant difference between the sorption performances of IMIP and INIP for the concentration range investigated. The effect of this relatively superior sorption performance of IMIP/INIP were investigated in more detail to find out whether the demonstrated any selectivity difference toward the analyte pyridoxal phosphate in presence of the related species.

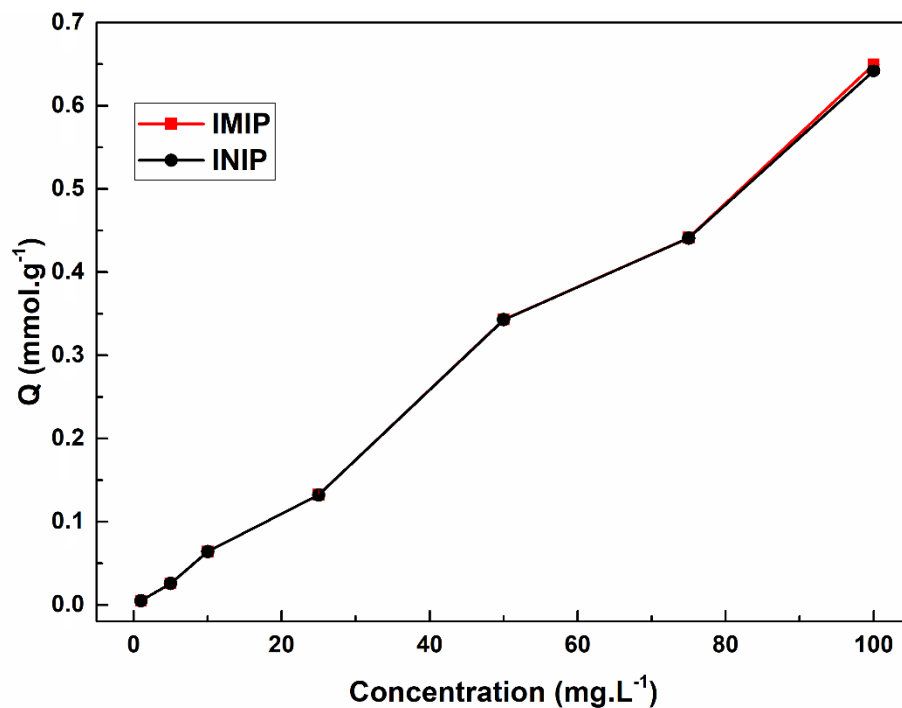


Figure 3.17. Sorption capacities of silica (sol-gel) based IMIP and INIP.

### 3.3.2 Selectivity Experiments

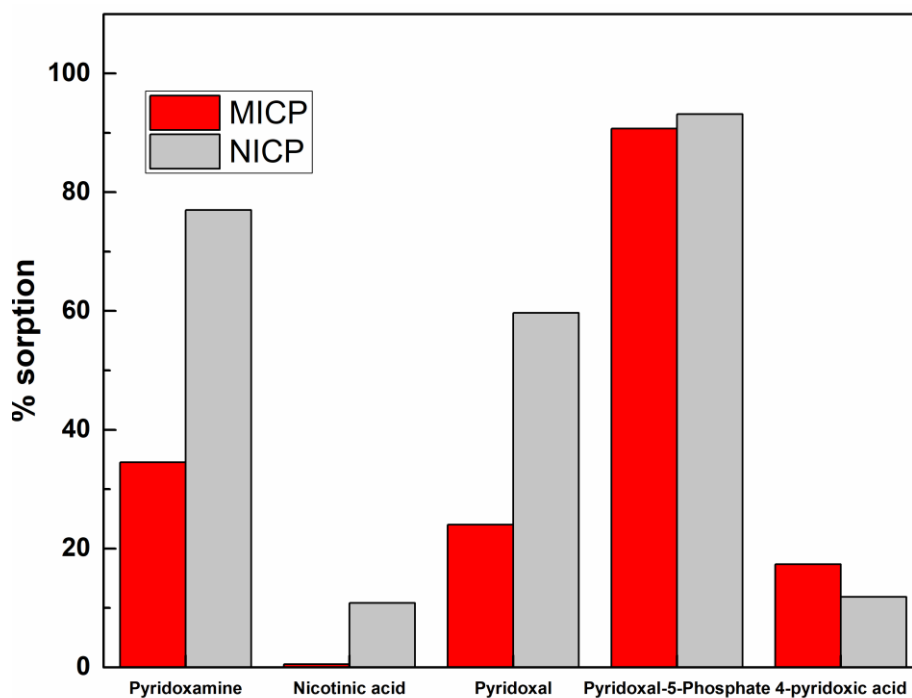


Figure 3.18. Sorption capacities of carbon sphere based MICP and NICK in the presence of pyridoxamine, nicotinic acid, pyridoxal and 4-pyridoxic acid.

The selectivity experiments were realized for the sorbents using the parameters mentioned in Section 2.6.2. Sorption capacities of MICP and NICP, MMICP and MNICP, IMIP and INIP for pyridoxal phosphate in the presence of pyridoxamine, nicotinic acid, pyridoxal and 4-pyridoxic acid are shown in Figure 3.18, Figure 3.19 and Figure 3.20, respectively.

The selectivity coefficients ( $K$ ) for the sorption of pyridoxal phosphate in the presence of competing species were calculated. The results are shown in Table 3.7 for MICP/NICP, in Table 3.8 for MMICP and MNICP, and in Table 3.9 for IMIP and INIP, as stated in Section 2.6.2.

Table. 3.7. Carbon sphere based MICP and NICP distribution coefficients, selectivity coefficients, and relative selectivity coefficients.

	<b>Pyridoxamine</b>	<b>Nicotinic acid</b>	<b>Pyridoxal</b>	<b>Pyridoxal phosphate</b>	<b>4-pyridoxic acid</b>
<b><math>K_d</math> MICP</b>	$5.27 \times 10^2$	5.00	$3.16 \times 10^2$	$9.77 \times 10^3$	$2.10 \times 10^2$
<b><math>K_d</math> NICP</b>	$3.35 \times 10^3$	$1.22 \times 10^2$	$1.48 \times 10^3$	$1.36 \times 10^4$	$1.35 \times 10^2$
<b><math>K</math> MICP</b>	18.5	$1.80 \times 10^3$	30.9	-	46.0
<b><math>K</math> NICP</b>	4.07	11.8	9.21	-	$1.01 \times 10^2$
<b><math>K'</math></b>	4.55	16.1	3.35	-	0.46

The distribution coefficients ( $K_d$ ) of pyridoxal phosphate, pyridoxamine, nicotinic acid, pyridoxal, and 4-pyridoxic acid were first computed. The distribution coefficients were used to calculate the selectivity coefficients for the pyridoxal phosphate/pyridoxamine couple (18.53 and 4.07 for MICP and NICP, respectively), the pyridoxal phosphate/nicotinic acid couple (1804.18 and 11.84 for MICP and NICP, respectively), the pyridoxal phosphate/pyridoxal couple (30.90 and 9.21 for MICP and NICP, respectively), and the pyridoxal phosphate/4-pyridoxic acid (46.03 and 101.3 for MICP and NICP, respectively). The reported data show that MICP (when compared to NICP) has an amazing relative selectivity to pyridoxal phosphate in the presence of nicotinic acid, with 16.13 times greater selectivity. The relative selectivity of MICP to pyridoxal phosphate in the presence of pyridoxamine and pyridoxal are 4.55 and 3.35,

respectively, compared to NICP. The structural similarities of these two compounds, as previously indicated, might explain MICP's lower selectivity for pyridoxal phosphate in the presence of 4-pyridoxic acid (only 0.46) compared to NICP.

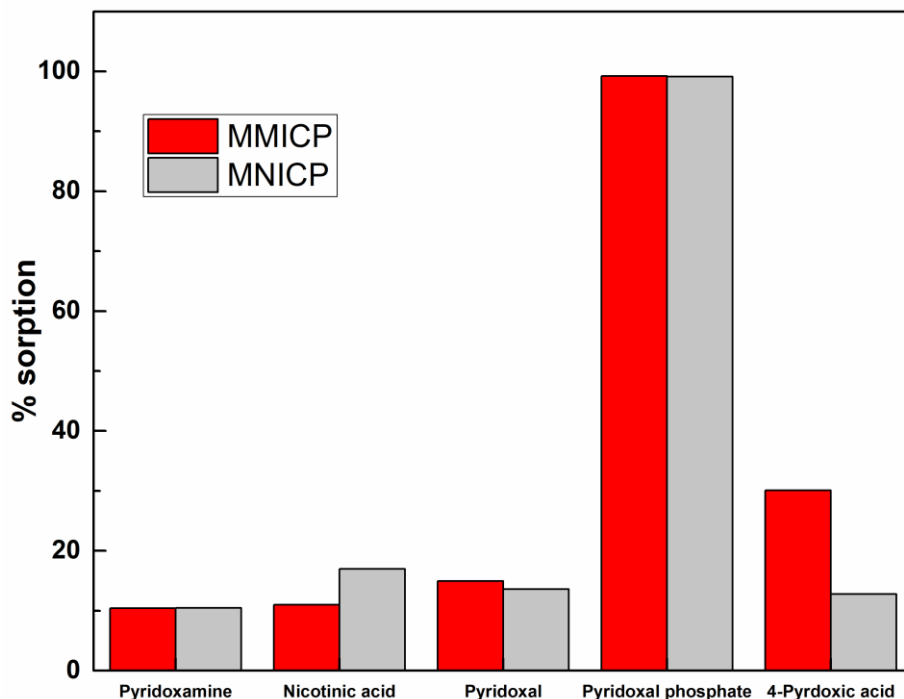


Figure 3.19. Sorption capacities of Fe<sub>3</sub>O<sub>4</sub> based MMICP and MNICP in the presence of pyridoxamine, nicotinic acid, pyridoxal and 4-pyridoxic acid.

The distribution coefficients were used to calculate the selectivity coefficients for the pyridoxal phosphate/pyridoxamine couple (1097.45 and 969.02 for MMICP and MNICP, respectively), the pyridoxal phosphate/nicotinic acid couple (1032.06 and 554.67 for MMICP and MNICP, respectively), the pyridoxal phosphate/pyridoxal couple (725.10 and 721.83 for MMICP and MNICP, respectively), and the pyridoxal phosphate/4-pyridoxic acid (296.32 and 776.06 for MMICP and MNICP, respectively). The reported data show that MMICP (when compared to MNICP) has a similar relative selectivity to pyridoxal phosphate in the presence of pyridoxamine, nicotinic acid, pyridoxal and 4-pyridoxic acid.

Table. 3.8. Fe<sub>3</sub>O<sub>4</sub> based MMICP and MNICP distribution coefficients, selectivity coefficients, and relative selectivity coefficients.

	Pyridoxamine	Nicotinic acid	Pyridoxal	Pyridoxal phosphate	4-pyridoxic acid
<b><i>K<sub>d</sub></i> MMICP</b>	1.16x10 <sup>2</sup>	1.23x10 <sup>2</sup>	1.76x10 <sup>2</sup>	1.27x10 <sup>5</sup>	2.43x10 <sup>3</sup>
<b><i>K<sub>d</sub></i> MNICP</b>	1.17x10 <sup>2</sup>	2.05x10 <sup>2</sup>	1.57x10 <sup>2</sup>	1.14x10 <sup>5</sup>	1.46x10 <sup>2</sup>
<b><i>K</i> MMICP</b>	1.10x10 <sup>3</sup>	1.03x10 <sup>3</sup>	7.25x10 <sup>2</sup>	-	2.96x10 <sup>2</sup>
<b><i>K</i> MNICP</b>	9.69x10 <sup>2</sup>	5.54x10 <sup>2</sup>	7.21x10 <sup>2</sup>	-	7.76x10 <sup>2</sup>
<b><i>K'</i></b>	1.13	1.86	1.00	-	0.38

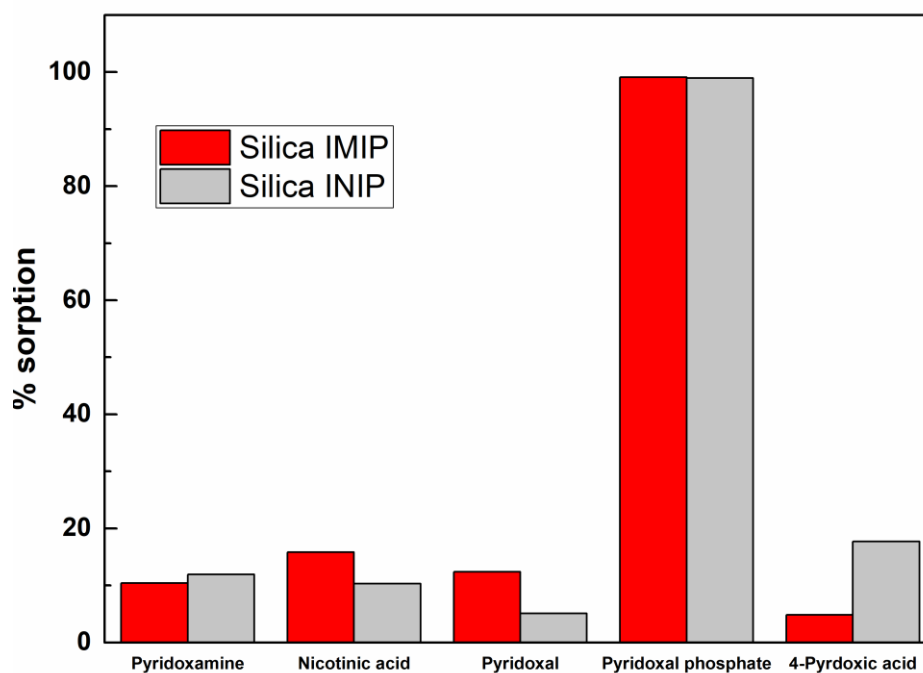


Figure 3.20. Sorption capacities of Silica (sol-gel) based IMIP and INIP in the presence of pyridoxamine, nicotinic acid, pyridoxal and 4-pyridoxic.

The distribution coefficients (*K<sub>d</sub>*) of pyridoxal phosphate, pyridoxamine, nicotinic acid, pyridoxal, and 4-pyridoxic acid were first computed. The distribution coefficients were used to calculate the selectivity coefficients for the pyridoxal phosphate/pyridoxamine couple (975.20 and 689.09 for IMIP and INIP, respectively), the

pyridoxal phosphate/nicotinic acid couple (602.40 and 811.99 for IMIP and INIP, respectively), the pyridoxal phosphate/pyridoxal couple (802.68 and 1736.18 for IMIP and INIP, respectively), and the pyridoxal phosphate/4-pyridoxal acid (2213.85 and 433.08 for IMIP and INIP, respectively). The reported data show that IMIP (when compared to INIP) has an amazing relative selectivity to pyridoxal phosphate in the presence of 4-pyridoxic acid, with 5.11 times greater selectivity. The relative selectivity of IMIP to pyridoxal phosphate in the presence of pyridoxamine, nicotinic acid and pyridoxal are 1.42, 0.74 and 0.46, respectively, compared to INIP. Both IMIP and INIP sorbents appear to be highly selective to pyridoxal phosphate in the presence of other species compared to other sorbents.

Table 3.9. Silica (sol-gel) based IMIP and INIP distribution coefficients, selectivity coefficients, and relative selectivity coefficients.

	<b>Pyridoxamine</b>	<b>Nicotinic acid</b>	<b>Pyridoxal</b>	<b>Pyridoxal phosphate</b>	<b>4-pyridoxic acid</b>
<b><math>K_d</math> IMIP</b>	$1.16 \times 10^2$	$1.89 \times 10^2$	$1.41 \times 10^2$	$1.1 \times 10^5$	51.0
<b><math>K_d</math> INIP</b>	$1.35 \times 10^2$	$1.15 \times 10^2$	54.0	$9.3 \times 10^4$	$2.15 \times 10^2$
<b><math>K</math> IMIP</b>	$9.75 \times 10^2$	$6.02 \times 10^2$	$8.03 \times 10^2$	-	$2.21 \times 10^3$
<b><math>K</math> INIP</b>	$6.89 \times 10^2$	$8.12 \times 10^2$	$1.74 \times 10^3$	-	$4.33 \times 10^2$
<b><math>K'</math></b>	1.42	0.74	0.46	-	5.11

### 3.3.3 Effect of Sorption Time

To evaluate the influence of shaking duration on pyridoxal phosphate sorption, 10.0 mg of sorbents (carbon sphere based MICP, Fe<sub>3</sub>O<sub>4</sub> based MMICP and silica (sol-gel) based IMIP) and 10.0 mL of sample solutions spiked to contain 5.0 mg.L<sup>-1</sup> pyridoxal phosphate were utilized. Extraction times of 5, 15, 30, 60, 120, 240, 480, 720, and 1440 minutes were examined with continuous agitation at 50 rpm.

Figure 3.21 displays the outcomes of this experiment. As seen in the figure, for IMIP and , maximum sorption (96%) is attained in 15 min. For MMICP, maximum sorption (95.8%) is reached in 240 min but it can be said that even 15 min will be

sufficient for a relatively high sorption (>94%). Among the three MIP-based sorbents, MICP requires a longer shaking time to reach maximum sorption. However, even 30 min can be used for a successful sorption provided that the system has been calibrated in advance.

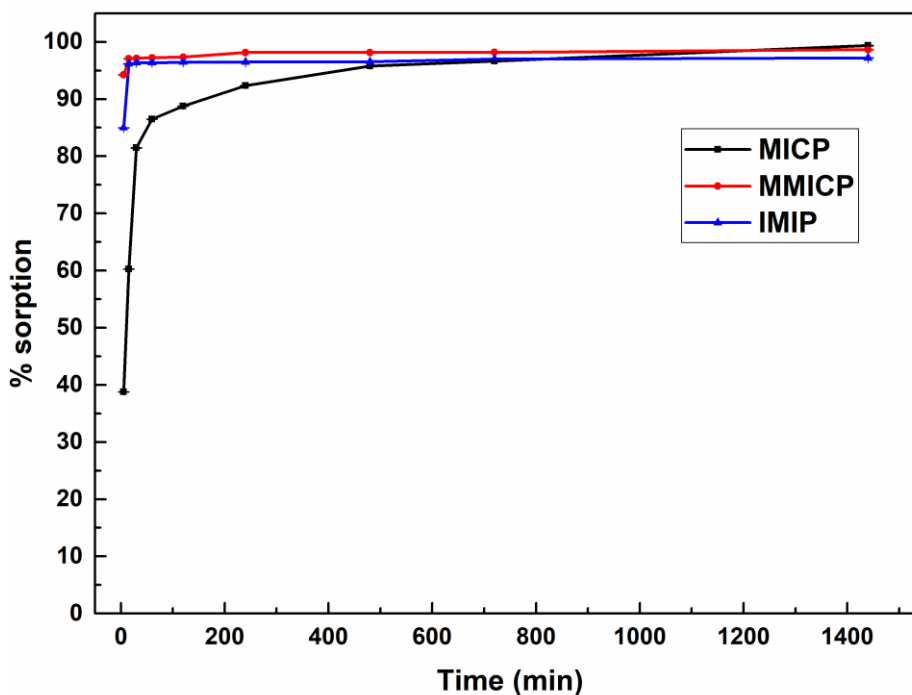


Figure 3.21. Effect of shaking time on the sorption of pyridoxal phosphate by carbon sphere based MICP, Fe<sub>3</sub>O<sub>4</sub> based MMICP and silica (sol-gel) based IMIP (n=3).

### 3.3.4 Effect of Sorbent Amount

For the investigation of sorbent amount effect on the sorption of pyridoxal phosphate, 0.5, 1.0, 3.0, 5.0 and 10.0 mg of the sorbents (MICP, MMICP and IMIP) were used. Sample volumes were 10.0 mL and the concentration of the samples were 5.0 mg.L<sup>-1</sup>. Sorption time was selected to be 24 h for the sake of comparison .

The outcome of the experiment is shown in Figure 3.22. From the figure, it can be said that the sorption behavior of MICP does not change while sorbent amount changes; even 0.5 mg of this sorbent is sufficient for a sorption percentage of around 95. On the other hand, the sorption percentage of MMICP and IMIP are increasing with

increasing sorbent amount. For MMICP, the maximum sorption was achieved at 5.0 mg for MMICP while it was 10.0 mg for IMIP.

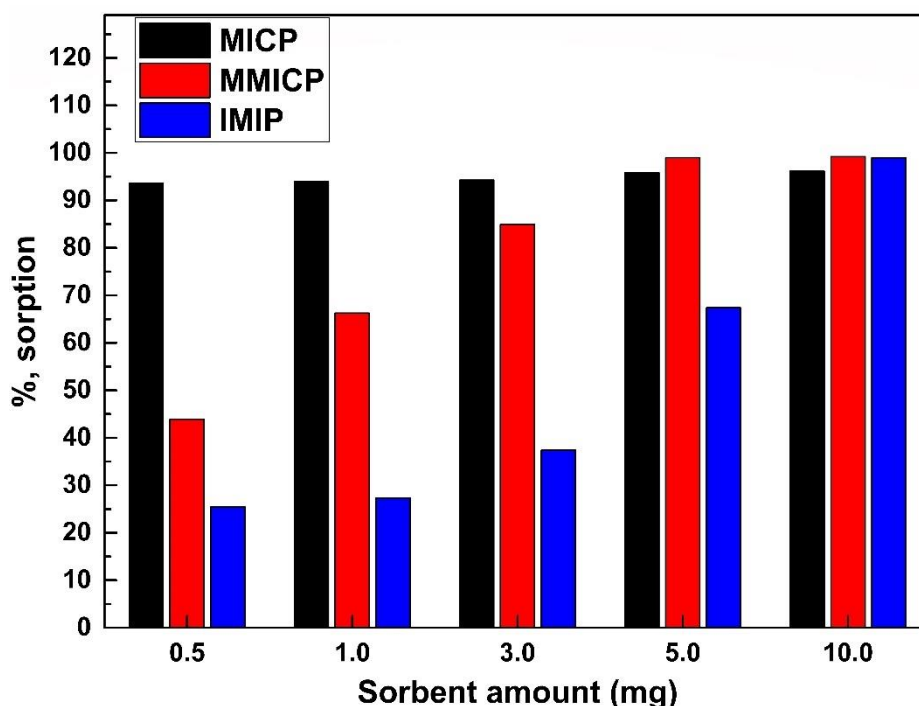


Figure 3.22. Effect of sorbent amounts on the sorption of pyridoxal phosphate by carbon sphere based MICP, Fe<sub>3</sub>O<sub>4</sub> based MMICP and silica (sol-gel) based IMIP (n=3).

### 3.3.5 Effect of Sample Volume

As indicated in Section 2.6.5, the influence of sample volumes on sorption percentage were examined for the three sorbents (MICP, MMICP and IMIP) with a sorbent amount of 5.0 mg and 24 h shaking time. Figure 3.23 demonstrates that after 10.0 mL of sample solution, the sorption percentage of the three sorbents decreases under the experimental conditions applied. At this point it can be mentioned that for 10.0 mL sample volume, 10.0 mg of the sorbents will be the optimum amount which guarantee higher than 98% sorption for MMICP and IMIP and higher than 95% sorption for MICP.

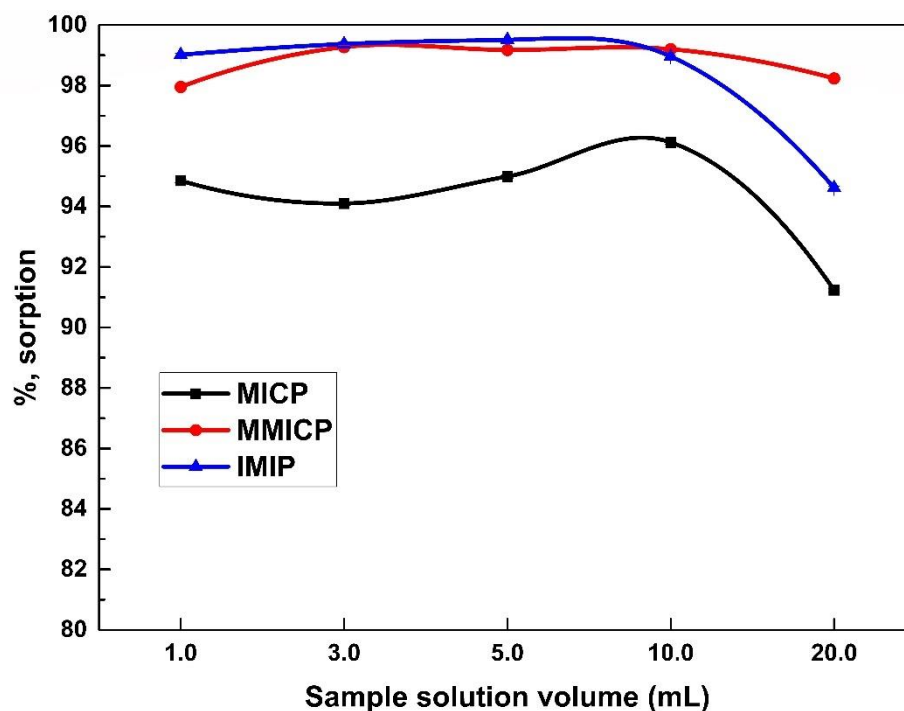


Figure 3.23. Effect of sample solution volumes on the sorption of pyridoxal phosphate by carbon sphere based MICP, Fe<sub>3</sub>O<sub>4</sub> based MMICP and silica (sol-gel)based IMIP, sorbent amount 10.0 mg, shaking time 24 h, (n=3).

### 3.4 Sorption Isotherm Models

The linear fits of the four types of isotherms were used to find the isotherm constants and specify the values of coefficients of determination ( $R^2$ ). The results are given in Table 3.10, Table 3.11 and Table 3.12. Relying solely on the  $R^2$  values to make judgement about the most appropriate isotherm model can be misleading in some cases. Based on this, the isotherm constants were inserted in the nonlinear isotherm equations and used to calculate the isotherm model values of  $Q$  corresponding to each concentration value of the sorbate. The obtained  $Q$  values were used to construct plots for each sorbent system containing experimental and model data, as shown in Figure 3.24. Moreover, the Chi-test was used to calculate the differences between the experimental and model values, in order to help decide about the best fitting isotherm, especially when the model curves show close behavior.

In the case of MICP and NICP, the curve plots in Fig.3.24 (a) and (b) in addition to the smaller values of variation between experimental and model data obtained from the Chi-tests, given in Table 3.13, show that the best fitting isotherm is the D-R isotherm.

Table 3.10. Summary of models' coefficients and constants for MICP and NICP.

<b>Adsorption model</b>	<b>Parameter</b>	<b>MICP</b>	<b>NICP</b>
<b>Langmuir</b>	Slope	48.72	52.82
	Intercept	-446.53	435.38
	R <sup>2</sup>	0.9876	0.9873
	$Q_{max}$ (mmol.g <sup>-1</sup> )	0.02	0.02
	$b$ (L.mmol <sup>-1</sup> )	9.17	8.24
<b>Freundlich</b>	Slope	1.94	1.79
	Intercept	0.33	9x10 <sup>-4</sup>
	R <sup>2</sup>	0.9897	0.9896
	$K_F$	2.14	1.00
	1/ $n$	0.52	0.56
<b>Dubinin-Radushkevich</b>	Slope	-9x10 <sup>-5</sup>	-8x10 <sup>-5</sup>
	Intercept	-1.06	-1.30
	R <sup>2</sup>	0.9785	0.9796
	B (mol <sup>2</sup> .kJ <sup>2</sup> )	9x10 <sup>-5</sup>	8x10 <sup>-5</sup>
	$q_s$ (mmol.g <sup>-1</sup> )	0.35	0.27
	E (kJ.mol <sup>-1</sup> )	74.5	79.1
<b>Harkins-Jura</b>	Slope	-6x10 <sup>-5</sup>	-7x10 <sup>-5</sup>
	Intercept	-1.56	-1.44
	R <sup>2</sup>	0.57	0.58
	$A$	16.7x10 <sup>3</sup>	1.43x10 <sup>3</sup>
	$B$	26.1x10 <sup>3</sup>	20.3x10 <sup>3</sup>

This isotherm model can usually be used to describe monolayer sorption of sorbates on heterogeneous surfaces, within intermediate concentration ranges. Heterogeneity may refer to sorption sites with different energies or different structure. Based on the adsorption capacity values calculated from the isotherm constant ( $Q_{max}$ ), provided in Table 3.10, it is concluded that MICP has a higher adsorption capacity than NICP. On the other hand, Freundlich isotherm seem to show some adequacy in the description of the

sorption data, in particular at smaller concentrations, while both of Langmuir and H-J isotherms are clearly not adequate for modelling the sorption data on both of sorbents, under the studied conditions.

Table 3.11. Summary of models' coefficients and constants for MMICP and NMICP.

<b>Adsorption model</b>	<b>Parameter</b>	<b>MMICP</b>	<b>NMICP</b>
<b>Langmuir</b>	Slope	48.09	51.08
	Intercept	$2.90 \times 10^3$	$0.69 \times 10^3$
	$R^2$	0.3593	0.6874
	$Q_{max}$ (mmol.g <sup>-1</sup> )	0.02	0.02
	$b$ (L.mmol <sup>-1</sup> )	60.4	13.5
<b>Freundlich</b>	Slope	1.89	1.80
	Intercept	-0.15	-0.75
	$R^2$	0.918	0.783
	$K_F$	0.70	0.18
	$1/n$	0.53	0.56
<b>Dubinin-Radushkevich</b>	Slope	$-6 \times 10^{-5}$	$-76 \times 10^{-5}$
	Intercept	-0.65	-0.99
	$R^2$	0.7985	0.9036
	$B$ (mol <sup>2</sup> .kJ <sup>2</sup> )	$6 \times 10^{-5}$	$7 \times 10^{-5}$
	$q_s$ (mmol.g <sup>-1</sup> )	0.52	0.37
	$E$ (kJ.mol <sup>-1</sup> )	91.3	84.5
<b>Harkins-Jura</b>	Slope	$-5 \times 10^{-5}$	$-6 \times 10^{-5}$
	Intercept	-2.34	-1.82
	$R^2$	0.21	0.38
	$A$	$2 \times 10^5$	$1.67 \times 10^5$
	$B$	$5.91 \times 10^5$	$3.01 \times 10^5$

In the case of MMICP and MNICP, and based on the curves in Fig. 3.24 (c) and (d), it seems that the best fitting isotherm model is Freundlich model. This model is appropriate for heterogeneous surfaces, but it allows for multilayer formation of the sorbate on the sorbent surface. From the values of the isotherm constant,  $K_F$  (given in Table 3.11), it can be concluded that the MMICP has higher sorption affinity toward the sorbate than MNICP. On the other hand, the other types of isotherm seem to yield values far from those obtained by experiment.

Table 3.12. Summary of models' coefficients and constants for IMIP and INIP.

Adsorption model	Parameter	MICP	NICP
<b>Langmuir</b>	Slope	28.77	24.99
	Intercept	$2.11 \times 10^3$	$1.80 \times 10^3$
	$R^2$	0.4255	0.4135
	$Q_{max}$ (mmol.g <sup>-1</sup> )	0.35	0.04
	$b$ (L.mmol <sup>-1</sup> )	73.47	71.90
<b>Freundlich</b>	Slope	0.97	0.93
	Intercept	-2.03	-2.17
	$R^2$	0.7631	0.7658
	$K_F$	$9.28 \times 10^{-3}$	$6.75 \times 10^{-3}$
	$1/n$	1.03	1.08
<b>Dubinin-Radushkevich</b>	Slope	$-1 \times 10^{-4}$	$-1 \times 10^{-4}$
	Intercept	1.05	0.85
	$R^2$	0.8003	0.8008
	$B$ (mol <sup>2</sup> .kJ <sup>2</sup> )	$1 \times 10^{-4}$	$1 \times 10^{-4}$
	$q_s$ (mmol.g <sup>-1</sup> )	2.87	2.34
	$E$ (kJ.mol <sup>-1</sup> )	70.7	70.7
<b>Harkins-Jura</b>	Slope	$-2 \times 10^{-5}$	$2 \times 10^{-5}$
	Intercept	-2.96	-2.85
	$R^2$	0.1873	0.1878
	$A$	$5 \times 10^5$	$5 \times 10^5$
	$B$	$1.48 \times 10^5$	$1.43 \times 10^5$

Finally, for IMIP and INIP, as the isotherm curves show in Fig 3.24 (e) and (f), poor correlation of the isotherm models with the experimental data is obtained in general, though a close correlation is seen only for the case of IMIP with Langmuir isotherm, under the studied conditions. This study can be extended by changing the concentration ranges and testing other types of isotherms.

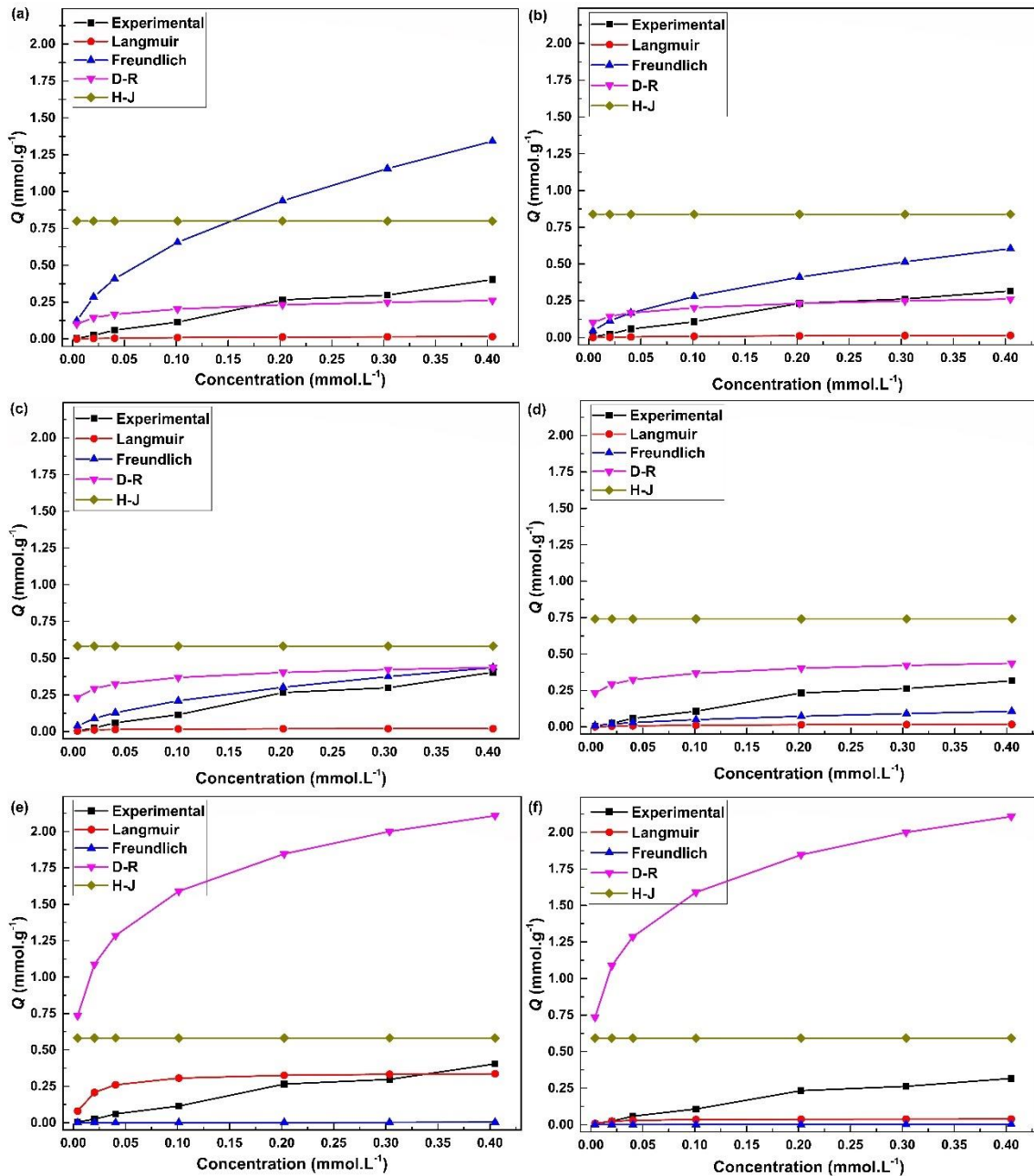


Figure 3.24. Nonlinear fit of isotherm models for sorption of pyridoxal phosphate by (a) MICP, (b) NICP, (c) MMICP, (d) NMICP, (e) IMIP and (f) INIP.

Table 3.13. Chi-tests results of MICP and NICP.

<b>MICP</b>				
	Langmuir	Freundlich	D-R	H-J
	0.03	0.11	0.09	0.79
	0.14	0.24	0.10	0.75
	0.54	0.30	0.07	0.68
	1.11	0.45	0.04	0.59
	4.77	0.48	0.00	0.36
	5.29	0.64	0.01	0.32
	9.31	0.66	0.08	0.20
<b>Sum</b>	<b>21.19</b>	<b>2.87</b>	<b>0.39</b>	<b>3.68</b>
<b>NICP</b>				
	Langmuir	Freundlich	D-R	H-J
	0.03	0.04	0.09	0.79
	0.18	0.07	0.10	0.75
	0.61	0.07	0.07	0.69
	1.13	0.11	0.05	0.60
	4.14	0.08	0.00	0.40
	4.60	0.12	0.00	0.36
	6.28	0.14	0.01	0.29
<b>Sum</b>	<b>16.97</b>	<b>0.62</b>	<b>0.32</b>	<b>3.88</b>

Table 3.14. Chi-tests results of MMICP and MNICP.

<b>MMICP</b>				
	Langmuir	Freundlich	D-R	H-J
	0.00	0.03	0.22	0.57
	0.02	0.05	0.25	0.53
	0.14	0.04	0.21	0.47
	0.54	0.04	0.17	0.38
	3.23	0.00	0.05	0.17
	4.00	0.02	0.04	0.14

(Continue on next page)

Table 3.14. (Cont.)

	7.54	0.00	0.00	0.05
Sum	15.46	0.18	0.94	2.31
<b>MNICP</b>				
	Langmuir	Freundlich	D-R	H-J
	0.02	0.00	0.22	0.73
	0.10	0.00	0.25	0.69
	0.38	0.03	0.22	0.63
	0.81	0.07	0.18	0.54
	3.33	0.35	0.07	0.35
	3.87	0.32	0.06	0.31
	5.44	0.41	0.03	0.24
Sum	13.95	1.18	1.03	3.50

Table 3.15. Chi-tests results of IMIP and INIP.

<b>IMIP</b>				
	Langmuir	Freundlich	D-R	H-J
	0.07	0.80	0.72	0.57
	0.16	3.61	1.04	0.53
	0.15	10.65	1.17	0.47
	0.12	14.85	1.37	0.38
	0.01	39.08	1.35	0.17
	0.00	32.15	1.45	0.14
	0.01	43.98	1.38	0.05
Sum	0.53	145.13	8.48	2.31
<b>INIP</b>				
	Langmuir	Freundlich	D-R	H-J
	0.00	1.40	0.72	0.58
	0.00	5.87	1.04	0.54
	0.03	15.86	1.17	0.48

(Continue on next page)

Table 3.12. (Cont.)

	0.15	19.88	1.38	0.40
	1.02	44.45	1.41	0.22
	1.32	36.41	1.51	0.18
	2.00	38.72	1.52	0.13
Sum	4.52	162.58	8.76	2.53

### 3.5 Desorption Studies

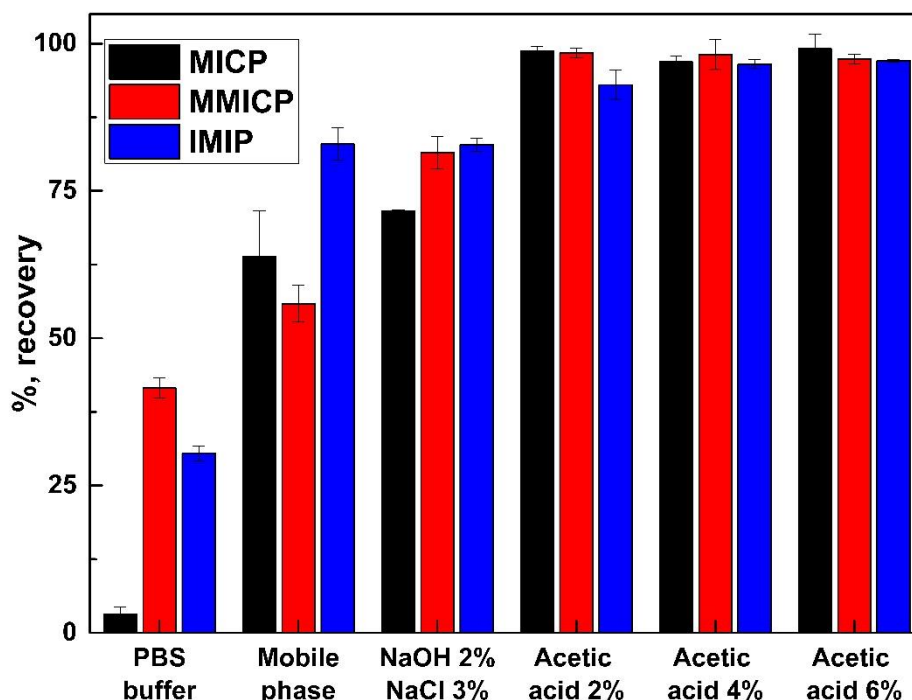


Figure 3.25. Effect of eluent type on desorption of pyridoxal phosphate from MICP, MMICP and IMIP.

Desorption experiments for MICP, MMICP, and IMIP were carried out as detailed in Section 2.8. The desorption percentages of several desorbing eluents are demonstrated in Figure 3.25. Among the investigated eluents, acetic acid solutions were determined to have the best elution performance, providing the highest percent recoveries for pyridoxal phosphate from all tested sorbents. It should be stated that MICP and MMICP chitosan were entirely dissolved in acetic acid solutions. A very high desorption percentage (97%) of previously adsorbed pyridoxal phosphate from MICP and MMICP sorbents can be

linked to the dissolution of chitosan in the eluents mentioned. The disturbance of hydrogen bonding between the analyte and the sorbent could be one of the reasons for this behavior. The other reason could be that acetate ions could swap places with analyte molecules resulting desorption of PLP from the sorbent. In the light of the desorption data, acetic acid (2%, v:v) solution was selected to be best for desorption of pyridoxal phosphate among the eluents tested.

### **3.6 Method Validation**

As method validation, the proposed MIP-SPE approaches were applied to various types of water and artificial serum samples spiked with pyridoxal phosphate using optimized sorption and desorption.

Before using the MIP-SPE approach, albumin was precipitated from synthetic serum samples. The precipitation procedure was utilized as stated in Section 2.9. Simply, methanol was added to the synthetic serum samples in such a volume so that the sample contained 50% methanol. Then, the mixture was centrifuged and albumin was precipitated. The sample solution was then separated from the precipitate. Finally, the sample solution that was freed from albumin was used in MIP-SPE.

The percent recoveries obtained after using the MIP-SPE approaches on various sample matrices are shown in Table 3.16. These findings clearly demonstrate that MIP recoveries are unaffected by matrix-to-matrix differences in different water types and may be utilized as a reliable approach for determining pyridoxal phosphate. Lower recoveries were seen in serum samples compared to water samples. The matrix modification with methanol conducted during protein precipitation might be the major cause of reduced recoveries. For the protein precipitation step, the organic solvent (methanol) that was added to the artificial serum samples was not removed. This treatment must have affected the analyte's affinity for the sorbents. On the other hand, the serum formulation 1 contained much less BSA than the formulation 2, so the protein precipitation might not occur completely in case of formulation 2 or some PLP still be bound to albumin. This may be the reason that all the sorbents showed poor recoveries for the analyte from formulation 2. As a result, if the approach is to be utilized for serum samples, the use of internal standards or matrix-matched calibration is advised.

Table 3.16. Recovery results obtained with the proposed method (n=3).

<b>% Recovery</b>		<b>Sorbents</b>		
<b>Samples</b>	<b>MICP</b>	<b>MMICP</b>	<b>IMIP</b>	
Ultra-pure water	98.7 ( $\pm 0.7$ )	98.4 ( $\pm 0.8$ )	92.9 ( $\pm 2.7$ )	
Bottled water	96.8 ( $\pm 1.1$ )	95.0 ( $\pm 1.3$ )	91.9 ( $\pm 1.2$ )	
Tap water	96.2 ( $\pm 1.5$ )	92.3 ( $\pm 1.5$ )	91.0 ( $\pm 1.3$ )	
Serum Formulation 1	84.0 ( $\pm 1.5$ )	84.1 ( $\pm 0.6$ )	80.1 ( $\pm 1.9$ )	
Serum Formulation 2	2.9 ( $\pm 0.8$ )	40.0 ( $\pm 3.9$ )	31.0 ( $\pm 1.9$ )	

## CHAPTER 4

### CONCLUSION

This study details a method for solid phase extraction of pyridoxal 5'-phosphate (PLP) using molecularly imprinted polymers synthesized through three different routes prior to HPLC determination.

In the first route, a carbon sphere based molecularly imprinted chitosan polymer (MICP) was synthesized using the procedure given in Ostovan et al. 2018. As a first step, chitosan was obtained via deacetylation of chitin (Boyacı et al. 2010) to chitosan. The degree of deacetylation of chitosan was determined by potentiometric titration and elemental analysis (>94% deacetylation). Carbon spheres were synthesized via hydrothermal carbonization from glucose as a carbon source. The carbon sphere based molecularly imprinted chitosan polymer was obtained by the precipitation of the mixture of chitosan, PLP and carbon spheres solution with NaOH solution.

In the second route, a Fe<sub>3</sub>O<sub>4</sub> based molecularly imprinted chitosan polymer (MMICP) was synthesized using the procedure given in Díaz-Hernández et al. 2018. The synthesis of the material was accomplished via co-precipitation of the mixture of Fe(II), Fe(III) and chitosan solution (prepared in first route) with NaOH solution in the presence of PLP.

In the third route, a sol-gel strategy was used to synthesize molecularly imprinted polymer (IMIP) using the procedure given in Shin 2013. PLP imprinted silica particles were obtained by the reaction of APTES as monomer and TEOS as crosslinker catalyzed with EtOH and NH<sub>3</sub>·H<sub>2</sub>O in the presence of PLP.

The characterization studies of the sorbents were done by using SEM, EDX, XRD and TGA. The morphology of the sorbents were investigated by SEM. The images of the MICP showed homogenous distribution of carbon sphere particles across the composite structure. In the MMICP images, it can be seen that the Fe<sub>3</sub>O<sub>4</sub> nano particles aggregated all over the composite structure. The homogeneous spherical particles of IMIP can be seen in the images of silica based MIPs. XRD data of the Fe<sub>3</sub>O<sub>4</sub> and Fe<sub>3</sub>O<sub>4</sub> based MIPs have demonstrated the successful preparation of Fe<sub>3</sub>O<sub>4</sub>-chitosan composite. EDX showed the elemental compositions of the materials. TGA results indicated that chitosan was successfully combined with Fe<sub>3</sub>O<sub>4</sub> nanoparticles. The 5.7% weight loss showed an

agreement with the weight ratio of chitosan in the composite, indicating a successful combination of chitosan and Fe<sub>3</sub>O<sub>4</sub> nanoparticles.

The sorption and optimization studies were done as stated in the relevant sections. The results indicated that carbon sphere-based molecularly imprinted chitosan polymer (MICP), magnetite based molecularly imprinted chitosan polymer (MMICP), and silica-based molecularly imprinted polymer (IMIP) may be used to successfully detain pyridoxal phosphate from various sample matrixes. For a sample volume of 10.0 mL and a shaking duration of 30 min, the optimum sorbent amounts were 5.0 mg for MICP, 10.0 mg for MMICP, and 10.0 mg for IMIP. Following the experimental optimization, the selectivity of the MIPs were also investigated against structurally similar compounds. In the presence of pyridoxamine, nicotinic acid, pyridoxal and 4-pyridoxic acid, all three sorbents shows selectivity towards PLP. Finally, for the desorption of PLP, acetic acid (2%, v/v) solution gave the best result among all of the eluents tested.

As a final study, developed MIP based methods were validated using spiked samples. Method validation showed that all the three methodologies utilizing different materials proposed in the thesis worked well for sorption of PLP for different water samples. In the case of synthetic serum samples, lower recoveries were obtained compared to the tested water samples, suggesting the sample matrix's importance in the compound's analysis. Furthermore, the two synthetic serum formulations had significantly different recoveries demonstrating a close relationship between the amount of protein in the sample and analyte recoveries. These findings highlight the importance of matrix-matched calibration for quantitative analyses of the analyte in such complex matrices.

## REFERENCES

- Alexander, Cameron, Håkan Andersson, Lars Andersson, Richard Ansell, Nicole Kirsch, Ian Nicholls, John O'Mahony, and Michael Whitcombe. 2006. "Molecular Imprinting Science and Technology: A Survey of the Literature for The Years Up to And Including 2003." *Journal of molecular recognition : JMR* 19:106-80. doi: 10.1002/jmr.760.
- Andersson, Lars, Börje Sellergren, Klaus Mosbach, and a. 1984. "Imprinting of amino acid derivatives in macroporous polymers." *Tetrahedron Letters* 25 (45):5211-5214. doi: [https://doi.org/10.1016/S0040-4039\(01\)81566-5](https://doi.org/10.1016/S0040-4039(01)81566-5).
- Augusto, Fabio, Leandro W. Hantao, Noroska G. S. Mogollón, and Soraia C. G. N. Braga. 2013. "New materials and trends in sorbents for solid-phase extraction." *TrAC Trends in Analytical Chemistry* 43:14-23. doi: <https://doi.org/10.1016/j.trac.2012.08.012>.
- Boyacı, Ezel, Ahmet E. Eroğlu, Talal Shahwan, and a. 2010. "Sorption of As(V) from waters using chitosan and chitosan-immobilized sodium silicate prior to atomic spectrometric determination." *Talanta* 80 (3):1452-1460. doi: <https://doi.org/10.1016/j.talanta.2009.09.053>.
- Burnouf, Thierry, and Mirjana Radosevich. 2001. "Affinity chromatography in the industrial purification of plasma proteins for therapeutic use." *Journal of biochemical and biophysical methods* 49:575-86. doi: 10.1016/S0165-022X(01)00221-4.
- Burton, Graham W., Anne Joyce, Keith U. Ingold, and a. 1983. "Is vitamin E the only lipid-soluble, chain-breaking antioxidant in human blood plasma and erythrocyte membranes?" *Archives of Biochemistry and Biophysics* 221 (1):281-290. doi: [https://doi.org/10.1016/0003-9861\(83\)90145-5](https://doi.org/10.1016/0003-9861(83)90145-5).
- Buszewski, Bogusław, and Malgorzata Szultka-Mlynska. 2012. "Past, Present, and Future of Solid Phase Extraction: A Review." *Critical Reviews in Analytical Chemistry - CRIT REV ANAL CHEM* 42:198-213. doi: 10.1080/07373937.2011.645413.
- Chen, L., S. Xu, J. Li, and a. 2011. "Recent advances in molecular imprinting technology: current status, challenges and highlighted applications." *Chem Soc Rev* 40 (5):2922-42. doi: 10.1039/c0cs00084a.
- Chen, Lingxin, Xiaoyan Wang, Wenhui Lu, Xiaqing Wu, and Jinhua Li. 2016. "Molecular imprinting: perspectives and applications." *Chemical Society Reviews* 45 (8):2137-2211. doi: 10.1039/C6CS00061D.
- Çiftçi, Tülin Deniz , and Yasemin İşlek Coşkun. 2020. "Removal of Pb(II) from Water Using (Fe<sub>3</sub>O<sub>4</sub>/Ni/NixB) Magnetic Nanocomposites, Carob (*Ceratonia siliqua*) or Grape Seeds (*Vitis vinifera*)." *Journal of Water Chemistry and Technology* 42 (3):185-195. doi: 10.3103/S1063455X2003011X.

- Díaz-Hernández, Azariel, Jorge Gracida, Blanca E. García-Almendárez, Carlos Regalado, Rosario Núñez, and Aldo Amaro-Reyes. 2018. "Characterization of Magnetic Nanoparticles Coated with Chitosan: A Potential Approach for Enzyme Immobilization." *Journal of Nanomaterials* 2018:9468574. doi: 10.1155/2018/9468574.
- Erdogan, Fatma Oguz. 2019. "Freundlich, Langmuir, Temkin, DR and Harkins-Jura Isotherm Studies on the Adsorption of CO<sub>2</sub> on Various Porous Adsorbents." *International Journal of Chemical Reactor Engineering* 17 (5). doi: doi:10.1515/ijcre-2018-0134.
- Farquharson, J., and J. F. Adams. 1976. "The forms of vitamin B12 in foods." *British Journal of Nutrition* 36 (1):127-136. doi: 10.1079/BJN19760063.
- Fattal-Valevski, Aviva. 2011. "Thiamine (Vitamin B1)." *Journal of Evidence-Based Complementary & Alternative Medicine* 16 (1):12-20. doi: 10.1177/1533210110392941.
- Fonda, M. L., C. Trauss, U. M. Guempel, and a. 1991. "The binding of pyridoxal 5'-phosphate to human serum albumin." *Arch Biochem Biophys* 288 (1):79-86. doi: 10.1016/0003-9861(91)90167-h.
- Goh, Su-Yen, and Mark E. Cooper. 2008. "The Role of Advanced Glycation End Products in Progression and Complications of Diabetes." *The Journal of Clinical Endocrinology & Metabolism* 93 (4):1143-1152. doi: 10.1210/jc.2007-1817 %J The Journal of Clinical Endocrinology & Metabolism.
- Gueu, S., B. Yao, K. Adouby, and G. Ado. 2007. "Kinetics and thermodynamics study of lead adsorption on to activated carbons from coconut and seed hull of the palm tree." *International Journal of Environmental Science & Technology* 4 (1):11-17. doi: 10.1007/BF03325956.
- Guibal, Eric, Céline Milot, and John Michael Tobin. 1998. "Metal-Anion Sorption by Chitosan Beads: Equilibrium and Kinetic Studies." *Industrial & Engineering Chemistry Research* 37 (4):1454-1463. doi: 10.1021/ie9703954.
- Hashim, S. N., R. I. Boysen, L. J. Schwarz, B. Danylec, and M. T. Hearn. 2014. "A comparison of covalent and non-covalent imprinting strategies for the synthesis of stigmasterol imprinted polymers." *J Chromatogr A* 1359:35-43. doi: 10.1016/j.chroma.2014.07.034.
- Haupt, Karsten, and Klaus Mosbach. 2000. "Molecularly Imprinted Polymers and Their Use in Biomimetic Sensors." *Chemical reviews* 100:2495-504. doi: 10.1021/cr990099w.
- Hennion, Marie-Claire. 1999. "Solid-phase extraction: method development, sorbents, and coupling with liquid chromatography." *Journal of Chromatography A* 856 (1):3-54. doi: https://doi.org/10.1016/S0021-9673(99)00832-8.
- Hongyuan, Yan, and Kyung Row. 2006. "Characteristic and Synthetic Approach of Molecularly Imprinted Polymer." *International Journal of Molecular Sciences* 7. doi: 10.3390/i7050155.

- Jiménez, M. Dolores Alvarez, M. Isabel Serrano Gil, M. Antonia Palacios Corvillo, and Luis Ma Polo Díez. 1988. "Determination of calcium and magnesium in milk by complexometric titration using protein precipitation and complexation with Palladiazole or other indicators." *Analyst* 113 (4):633-635. doi: <https://doi.org/10.1039/AN9881300633>.
- Karrat, Abdelhafid, Abderrahman Lamaoui, Aziz Amine, Jose Palacios Santander, and Laura Cubillana-Aguilera. 2020. "Applications of Chitosan in Molecularly and Ion Imprinted Polymers." *Chemistry Africa* 3. doi: 10.1007/s42250-020-00177-w.
- Karrat, Abdelhafid, José María Palacios-Santander, Aziz Amine, and Laura Cubillana-Aguilera. 2022. "A novel magnetic molecularly imprinted polymer for selective extraction and determination of quercetin in plant samples." *Analytica Chimica Acta* 1203:339709. doi: <https://doi.org/10.1016/j.aca.2022.339709>.
- Kasaai, Mohammad Reza, Joseph Arul, Gérard Charlet, and a. 2000. "Intrinsic viscosity—Molecular weight relationship for chitosan." *Journal of Polymer Science Part B: Polymer Physics* 38:2591-2598. doi: 10.1002/1099-0488(20001001)38:19<2591::AID-POLB110>3.0.CO;2-6.
- Kavitha, D., and C. Namasivayam. 2007. "Recycling coir pith, an agricultural solid waste, for the removal of Procion Orange from wastewater." *Dyes and Pigments - DYE PIGMENT* 74:237-248. doi: 10.1016/j.dyepig.2006.01.040.
- Kempe, Maria, Klaus Mosbach, a, and b. 1995. "Separation of amino acids, peptides and proteins on molecularly imprinted stationary phases." *Journal of Chromatography A* 691 (1):317-323. doi: [https://doi.org/10.1016/0021-9673\(94\)00820-Y](https://doi.org/10.1016/0021-9673(94)00820-Y).
- Kharroubi, M., F. Bellali, A. Karrat, M. Bouchdoug, and A. Jaouad. 2021. "Preparation of Teucrium polium extract-loaded chitosan-sodium lauryl sulfate beads and chitosan-alginate films for wound dressing application." *AIMS Public Health* 8 (4):754-775. doi: 10.3934/publichealth.2021059.
- Kimura, Mieko, Kazunori Kanehira, and Katsuhiko Yokoi. 1996. "Highly sensitive and simple liquid chromatographic determination in plasma of B6 vitamers, especially pyridoxal 5'-phosphate." *Journal of Chromatography A* 722 (1):295-301. doi: [https://doi.org/10.1016/0021-9673\(95\)00354-1](https://doi.org/10.1016/0021-9673(95)00354-1).
- Kongsbak, K., S. H. Thilsted, M. A. Wahed, and a. 2008. "Effect of consumption of the nutrient-dense, freshwater small fish *Amblypharyngodon mola* on biochemical indicators of vitamin A status in Bangladeshi children: a randomised, controlled study of efficacy." *Br J Nutr* 99 (3):581-97. doi: 10.1017/s000711450781912x.
- Lanska, D. J. 2012. "The Discovery of Niacin, Biotin, and Pantothenic Acid." *Annals of Nutrition and Metabolism* 61 (3):246-253. doi: 10.1159/000343115.
- Limousin, G., J. P. Gaudet, L. Charlet, S. Szenknect, V. Barthès, and M. Krimissa. 2007. "Sorption isotherms: A review on physical bases, modeling and measurement." *Applied Geochemistry* 22 (2):249-275. doi: <https://doi.org/10.1016/j.apgeochem.2006.09.010>.

- Liu, Weifeng, Lei Qin, Weiping Shi, Lin Chen, Yongzhen Yang, Xuguang Liu, and Bingshe Xu. 2016. "Molecularly imprinted polymers on the surface of porous carbon microspheres for capturing dibenzothiophene." *Microchimica Acta* 183. doi: 10.1007/s00604-016-1746-2.
- Mann, Dudley L, George M Ware, Evelyn Bonnin, Ronald R Eitenmiller, and Collaborators:. 2019. "Liquid Chromatographic Analysis of Vitamin B6 in Reconstituted Infant Formula: Collaborative Study." *Journal of AOAC INTERNATIONAL* 88 (1):30-37. doi: 10.1093/jaoac/88.1.30 %J Journal of AOAC INTERNATIONAL.
- Medicine, Institute of. 1998. *Dietary Reference Intakes for Thiamin, Riboflavin, Niacin, Vitamin B6, Folate, Vitamin B12, Pantothenic Acid, Biotin, and Choline*. Washington, DC: The National Academies Press.
- Nakamura, S., and T. Niwa. 2005. "Pyridoxal phosphate and hepatocyte growth factor prevent dialysate-induced peritoneal damage." *J Am Soc Nephrol* 16 (1):144-50. doi: 10.1681/asn.2004020120.
- Nur Hasanah, Aliya, Nisa Safitri, Aulia Zulfa, Neli Neli, and Driyanti Rahayu. 2021. "Factors Affecting Preparation of Molecularly Imprinted Polymer and Methods on Finding Template-Monomer Interaction as the Key of Selective Properties of the Materials." *Molecules* 26:5612. doi: 10.3390/molecules26185612.
- Ostovan, A., M. Ghaedi, M. Arabi, Q. Yang, J. Li, and L. Chen. 2018. "Hydrophilic Multitemplate Molecularly Imprinted Biopolymers Based on a Green Synthesis Strategy for Determination of B-Family Vitamins." *ACS Appl Mater Interfaces* 10 (4):4140-4150. doi: 10.1021/acsami.7b17500.
- Padayatty, S. J., A. Katz, Y. Wang, P. Eck, O. Kwon, J. H. Lee, S. Chen, C. Corpe, A. Dutta, S. K. Dutta, and M. Levine. 2003. "Vitamin C as an antioxidant: evaluation of its role in disease prevention." *J Am Coll Nutr* 22 (1):18-35. doi: 10.1080/07315724.2003.10719272.
- Priehl, B., G. Treiber, T. R. Pieber, and K. Amrein. 2013. "Vitamin D and immune function." *Nutrients* 5 (7):2502-21. doi: 10.3390/nu5072502.
- Qi, Lifeng, and Zirong Xu. 2004. "Lead sorption from aqueous solutions on chitosan nanoparticles." *Colloids and Surfaces A: Physicochemical and Engineering Aspects* 251 (1):183-190. doi: <https://doi.org/10.1016/j.colsurfa.2004.10.010>.
- Qin, Lei, Xiaorui Jia, Yongzhen Yang, and Xuguang Liu. 2016. "Porous Carbon Microspheres: An Excellent Support To Prepare Surface Molecularly Imprinted Polymers for Selective Removal of Dibenzothiophene in Fuel Oil." *Industrial & Engineering Chemistry Research* 55 (6):1710-1719. doi: 10.1021/acs.iecr.5b02837.
- Raeke, Julia, Oliver J. Lechtenfeld, Martin Wagner, Peter Herzprung, and Thorsten Reemtsma. 2016. "Selectivity of solid phase extraction of freshwater dissolved organic matter and its effect on ultrahigh resolution mass spectra." *Environmental Science: Processes & Impacts* 18 (7):918-927. doi: 10.1039/C6EM00200E.

- Rhee, S. Y., and Y. S. Kim. 2018. "The Role of Advanced Glycation End Products in Diabetic Vascular Complications." *Diabetes Metab J* 42 (3):188-195. doi: 10.4093/dmj.2017.0105.
- Sajini, T., and Beena Mathew. 2021. "A brief overview of molecularly imprinted polymers: Highlighting computational design, nano and photo-responsive imprinting." *Talanta Open* 4:100072. doi: <https://doi.org/10.1016/j.talo.2021.100072>.
- Sharma, U., D. Pal, R. Prasad, and a. 2014. "Alkaline phosphatase: an overview." *Indian J Clin Biochem* 29 (3):269-78. doi: 10.1007/s12291-013-0408-y.
- Shin, Min. 2013. "Inorganic Molecularly Imprinted Polymer by Sol-Gel Process for Recognition of Caffeine." *Open Journal of Organic Polymer Materials* 03:1-5. doi: 10.4236/ojopm.2013.31001.
- Spinneker, A., R. Sola, V. Lemmen, M. J. Castillo, K. Pietrzik, and M. González-Gross. 2007. "Vitamin B6 status, deficiency and its consequences--an overview." *Nutr Hosp* 22 (1):7-24.
- Srivastava, Satish K., and Ernest Beutler. 1973. "A new fluorometric method for the determination of pyridoxal 5'-phosphate." *Biochimica et Biophysica Acta (BBA) - General Subjects* 304 (3):765-773. doi: [https://doi.org/10.1016/0304-4165\(73\)90223-7](https://doi.org/10.1016/0304-4165(73)90223-7).
- Şeker, Ayşegül, Talal Shahwan, Ahmet E. Eroğlu, Sinan Yılmaz, Zeliha Demirel, and Meltem Conk Dalay. 2008. "Equilibrium, thermodynamic and kinetic studies for the biosorption of aqueous lead(II), cadmium(II) and nickel(II) ions on *Spirulina platensis*." *Journal of Hazardous Materials* 154 (1):973-980. doi: <https://doi.org/10.1016/j.jhazmat.2007.11.007>.
- Tahiliani, Arun G., and Cathy J. Beinlich. 1991. "Pantothenic Acid in Health and Disease" Dedicated to the late Dr. James R. Neely." In *Vitamins & Hormones*, edited by G. D. Aurbach, 165-228. Academic Press.
- Tolaimate, A., J. Desbrières, M. Rhazi, A. Alagui, M. Vincendon, and P. Vottero. 2000. "On the influence of deacetylation process on the physicochemical characteristics of chitosan from squid chitin." *Polymer* 41 (7):2463-2469. doi: [https://doi.org/10.1016/S0032-3861\(99\)00400-0](https://doi.org/10.1016/S0032-3861(99)00400-0).
- Ueland, Per Magne, Adrian McCann, Øivind Midttun, and Arve Ulvik. 2017. "Inflammation, vitamin B6 and related pathways." *Molecular Aspects of Medicine* 53:10-27. doi: <https://doi.org/10.1016/j.mam.2016.08.001>.
- Ueland, Per Magne, Arve Ulvik, Luisa Rios-Avila, Øivind Midttun, and Jesse F. Gregory. 2015. "Direct and Functional Biomarkers of Vitamin B6 Status." *Annual Review of Nutrition* 35 (1):33-70. doi: 10.1146/annurev-nutr-071714-034330.
- Umpleby, Robert J., Sarah C. Baxter, Miguel Bode, John K. Berch, Ripal N. Shah, and Ken D. Shimizu. 2001. "Application of the Freundlich adsorption isotherm in

- the characterization of molecularly imprinted polymers." *Analytica Chimica Acta* 435 (1):35-42. doi: [https://doi.org/10.1016/S0003-2670\(00\)01211-3](https://doi.org/10.1016/S0003-2670(00)01211-3).
- Uygun, Zihni Onur, and Mustafa Kemal Sezgintürk. 2011. "A novel, ultra sensible biosensor built by layer-by-layer covalent attachment of a receptor for diagnosis of tumor growth." *Analytica Chimica Acta* 706 (2):343-348. doi: <https://doi.org/10.1016/j.aca.2011.08.044>.
- Vermeer, C. 2012. "Vitamin K: the effect on health beyond coagulation - an overview." *Food Nutr Res* 56. doi: [10.3402/fnr.v56i0.5329](https://doi.org/10.3402/fnr.v56i0.5329).
- Wikipedia. 2021, 10 January, 15:35 UTC. "Pyridoxal phosphate." Wikipedia, The Free Encyclopedia., Last Modified 7 December 2020 00:19 UTC, accessed 10 January 2021 15:35 UTC. [https://en.wikipedia.org/w/index.php?title=Pyridoxal\\_phosphate&oldid=992768942](https://en.wikipedia.org/w/index.php?title=Pyridoxal_phosphate&oldid=992768942).
- Wulff, G. 1982. "Selective binding to polymers via covalent bonds. The construction of chiral cavities as specific receptor sites." *Pure and Applied Chemistry* 54 (11):2093-2102. doi: <https://doi.org/10.1351/pac198254112093>.
- Xu, Long, Yun-An Huang, Qiu-Jin Zhu, and Chun Ye. 2015. "Chitosan in Molecularly-Imprinted Polymers: Current and Future Prospects." *International Journal of Molecular Sciences* 16 (8). doi: [10.3390/ijms160818328](https://doi.org/10.3390/ijms160818328).
- Yavuz, Handan, Rıdvan Say, Adil Denizli, and a. 2005. "Iron removal from human plasma based on molecular recognition using imprinted beads." *Materials Science and Engineering: C* 25 (4):521-528. doi: <https://doi.org/10.1016/j.msec.2005.04.005>.
- Zheng, Hangyu, and Masakazu Yoshikawa. 2015. "Molecularly imprinted cellulose membranes for pervaporation separation of xylene isomers." *Journal of Membrane Science* 478:148-154. doi: <https://doi.org/10.1016/j.memsci.2014.12.048>.